Journal of Macromolecular Science, Part A
Publication details, including instructions for authors and subscription information:
http://www.informaworld.com/smpp/title~content=t713597274

Mathematical Modeling of Acrylonitrile-Butadiene Emulsion Copolymerization: Model Development and Validation

I. D. Washington[a]; T. A. Duever[a]; A. Penlidis[a]
[a] Institute for Polymer Research (IPR), Department of Chemical Engineering, University of Waterloo, Waterloo, Canada

Online publication date: 05 July 2010

To cite this Article Washington, I. D. , Duever, T. A. and Penlidis, A.(2010) 'Mathematical Modeling of Acrylonitrile-Butadiene Emulsion Copolymerization: Model Development and Validation', Journal of Macromolecular Science, Part A, 47: 8, 747 — 769
To link to this Article: DOI: 10.1080/10601325.2010.491436
URL: http://dx.doi.org/10.1080/10601325.2010.491436

Journal of Macromolecular Science, Part A: Pure and Applied Chemistry (2010) **47**, 747–769

ISSN: 1060-1325 print / 1520-5738 online
DOI: 10.1080/10601325.2010.491436

Taylor & Francis
Taylor & Francis Group

Mathematical Modeling of Acrylonitrile-Butadiene Emulsion Copolymerization: Model Development and Validation

I.D. WASHINGTON, T.A. DUEVER and A. PENLIDIS*

Institute for Polymer Research (IPR), Department of Chemical Engineering, University of Waterloo, Waterloo, Canada

Received, Accepted February 2010

This paper presents a mechanistic model for the production of nitrile-butadiene rubber (NBR). The mathematical dynamic model was developed in order to simulate the industrial production of NBR via emulsion copolymerization of acrylonitrile (AN) and butadiene (Bd) in batch, continuous and trains of continuous reactors. For this reason, the model was constructed in a parsimonious manner to avoid complex and time-consuming computations that typically result when modeling details of specific aspects of micro/macro scale emulsion polymerization phenomena (i.e., full molecular weight and particle size distributions, detailed species phase-partitioning, etc.). Thus, the model provides average properties for typical emulsion characteristics, such as monomer conversion, copolymer composition, number- and weight-average molecular weights, tri- and tetra-functional branching frequencies, and the number and average size of polymer latex particles. The proposed model is an extension of a previous model developed by our group, and allows for the dynamic modeling of different reactor types and configurations. Model comparisons are made between limited literature data for batch operation, while representative simulation profiles are shown for a reactor train.

Keywords: Dynamic modeling, emulsion copolymerization, batch/continuous reactors, continuous reactor train, nitrile-butadiene rubber, acrylonitrile-butadiene.

Nomenclature

A_1, A_2, A_3	=	Parameters for the termination rate constant expression
A_m, A_p	=	Total free micellar area; total particle phase surface area (dm^2)
$\overline{BN}_3$, $\overline{BN}_4$	=	Average number of tri- and tetra-functional branches per chain (#/molecule)
C_{fm}, C_{fp}, C_{fcta}, C_{fmsi}, C_{p^*}, $C_{p^{**}}$	=	Overall transfer coefficient for transfer to monomer, polymer, and CTA, reaction with impurities, internal and terminal double bond polymerization (e.g., for transfer to monomer $C_{fm} = k_{fm}/k_p$)
CMC_i	=	Critical micelle concentration for emulsifier i (mol/L)
$\bar{d}_p$	=	Average (swollen) particle diameter (dm)
$[E]_o$	=	Total emulsifier concentration initially in a batch reactor or in the feed to a continuous reactor (mol/L)
$[E_i]_a$	=	Concentration of emulsifier i in the reactor (mol/L)
$\bar{F}_{AN}$	=	Cumulative copolymer composition of AN
f	=	Initiator efficiency
$F_{i_{in}}$	=	Total molar inflow of species i = I, RA, Fe, Fe^{2+}, Fe^{3+}, m_j, pol_j, m_{ja}, w, e_j, wsi_j, msi_j, cta_j (mol/min)
F_i	=	Total molar outflow of species i = I, RA, Fe, Fe^{2+}, Fe^{3+}, m_j, pol_j, m_{ja}, w, e_j, wsi_j, msi_j, cta_j (mol/min)
growth	=	Rate of increase of the particle phase volume (L/min)
G	=	Polymer production rate (kg/min)
H	=	Homogeneous nucleation coefficient (dm^3)

*Address correspondence to: A. Penlidis, Institute for Polymer Research (IPR), Department of Chemical Engineering, University of Waterloo, Waterloo, ON N2L 3G1, Canada. E-mail: penlidis@cape.uwaterloo.ca

$[I]_o$ = Total initiator concentration initially in a batch reactor or in the feed to a continuous reactor (mol/L)

j_{cr} = Overall critical radical chain length at which radical precipitate from solution (#)

k_{cm} = Micelle radical capture rate constant (dm/min)

k_{cp} = Particle radical capture rate constant (dm/min)

k_{des} = Radical desorption rate constant (1/min)

k_{fcta_A}, k_{fcta_B} = Transfer to chain transfer agent rate constant between CTA and a radical ending in monomer A (B) (L/mol/min)

$k_{fm_{AA}}, k_{fm_{BB}}$ = Transfer to monomer rate constant between monomer A (B) and a radical ending in monomer A (B) (L/mol/min)

$k_{fm_{AB}}, k_{fm_{BA}}$ = Transfer to monomer rate constant between monomer B (A) and a radical ending in monomer A (B) (L/mol/min)

$k_{fp_{AB}}, k_{fp_{BA}}$ = Transfer to polymer rate constant between monomer B (A) and a radical ending in monomer A (B) (L/mol/min)

k_{fp_k} = Overall pseudo transfer to polymer rate constant in phase k (L/mol/min)

k_{fx_k} = Overall pseudo transfer to impurity or CTA rate constant in phase k (L/mol/min)

k_h, k_{h_o} = Homogeneous nucleation rate constant (1/min)

$K_i^{a/p}$ = Partition coefficient for species i between the aqueous and particle phases

$K_i^{d/p}$ = Partition coefficient for species i between the droplet and particle phases

$k_{p_{AA}}, k_{p_{BB}}$ = Propagation rate constant between monomer A (B) and a radical ending in monomer A (B) (L/mol/min)

$k_{p_{AA}}^{**}, k_{p_{BB}}^{**}$ = Reaction with internal bond rate constant between monomer A (B) in the polymer chain and a radical ending in monomer A (B) (L/mol/min)

$k_{p_{AB}}, k_{p_{BA}}$ = Cross-propagation rate constant between monomer B (A) and a radical ending in monomer A (B) (L/mol/min)

$k_{p_{AB}}^{**}, k_{p_{BA}}^{**}$ = Reaction with internal bond rate constant between monomer B (A) in the polymer chain and a radical ending in monomer A (B) (L/mol/min)

k_{p_k} = Overall pseudo propagation rate constant in phase k (L/mol/min)

$k_{t_{0_p}}$ = Overall termination rate constant at zero conversion (L/mol/min)

$k_{t_{AA}}, k_{t_{BB}}$ = Termination monomer rate constant between monomer A (B) and a radical ending in monomer A (B) (L/mol/min)

k_{t_p} = Overall termination rate constant in the particle phase (L/mol/min)

L = Critical average diffusion path length of a free radical in the aqueous phase before precipitation (dm)

$[M]_k$ = Total monomer concentration in phase k (mol/L)

$\bar{M}_n, \bar{M}_w$ = Cumulative number- and weight-average molecular weight (g/mol)

M_i = Mass of species i, where $i = \mathrm{pol}_j, \mathrm{m}_j$, w, e_j (g)

MW_{m_j} = Molecular weight of monomer j (g/mol)

MWD = Molecular weight distribution

$\bar{n}$ = Average number of radicals per particle (#/#)

N_A = Avogadro's number (#/mol)

N_i = Total moles of species i = I, RA, Fe, Fe^{2+}, Fe^{3+}, m_j, pol_j, m_{ja}, w, e_j, wsi_j, msi_j, cta_j

$N_{m,em,x}$ = Number of monomers (m), emulsifiers (em) or other species (x)

$N_{m_{i_p}}, N_{m_{i_d}}$ = Total moles of monomer in the particle and droplet phases (mol)

N_p = Number of polymer particles (#)

p = Dimensionless group representing radical loss from particles by either desorption or reaction with impurities

PDI = Poly-dispersity index ($\bar{M}_w/\bar{M}_n$)

q_k = Volumetric flow rate of phase k (k = a,p,d) out of the reactor (L/min)

$q_{T_{in}}, q_T$ = Total volumetric flow rate in/out of the reactor (L/min)

$[R^{\cdot}_{j_{cr}}]_a$ = Concentration of radicals in the aqueous phase at the critical chain length (j_{cr}) (mol/L)

$[R^{\cdot}]_a$ = Total concentration of radicals in the aqueous phase (mol/L)

$[R^{\cdot}]_a^{des}$ = Concentration of desorbed radicals in the aqueous phase capable of being recaptured by particles (mol/L)

$[R^{\cdot}]_a^{hom}$ = Concentration of radicals in the aqueous phase capable of undergoing homogeneous nucleation (mol/L)

$[R^{\cdot}]_a^{mic}$ = Concentration of radicals in the aqueous phase capable of being captured by micelles (mol/L)

$[R^{\cdot}]_a^{par}$ = Concentration of radicals in the aqueous phase capable of being captured by particles (mol/L)

$[R^{\cdot}]_p$ = Total concentration of radicals in the particle phase (mol/L)
$[R^{\cdot}_{in}]_a$ = Concentration of initiator fragment radicals in the aqueous phase (mol/L)
$[R^{\cdot}_k]_a, [R^{\cdot}_{k,i}]_a$ = Concentration of radicals in the aqueous phase of length k (mol/L)
r_A, r_B = Reactivity ratios for AN and Bd
$R_{cta_{jp}}$ = Rate of chain transfer agent consumption (mol/L/min)
R^{mic}_{des} = Rate of recapture of desorbed radicals by micelles (#/L/min)
R_{I_c} = Rate of initiator consumption (mol/L/min)
R_{i_k} = Rate of consumption or generation of species i in phase k (mol/L/min)
R_I = Rate of initiation (mol/L/min)
r_{mic} = Average micelle radius (dm)
R_{mic}, R_{hom} = Rate of micellar and homogeneous nucleation (#/L/min)
$R_{p_{j_k}}$ = Rate of polymerization of monomer j in phase k (mol/L/min)
$R_{p_{jp}}$, $R_{p_{ja}}$ = Rates of polymerization in particle and aqueous phases (mol/L/min)
R_{RA}, $R_{Fe^{2+}}$, $R_{Fe^{3+}}$ = Rates of redox ingredient consumption (mol/L/min)
$R_{V_pQ_0\overline{BN}_i}$ = Rate of $\overline{BN}_i$ generation for $i = 3, 4$ (mol/L/min)
$R_{V_pQ_i}$ = Rate of moment generation for moments $i = 0, 1, 2$ (mol/L/min)
$R_{wsi_{jp}}$, $R_{msi_{jp}}$ = Rates of impurity consumption (mol/L/min)
shrinkage = Rate of decrease of the organic phase volume (i.e., droplet and particle phases) (L/min)
S_a = Surface area covered by one molecule of emulsifier (dm^2/molecule)
SAN = Styrene acrylonitrile copolymer
SBR = Styrene butadiene rubber
transfer_j = Rate of monomer transfer from the aqueous to particle phase (mol/min)
V_a = Volume of the aqueous phase (i.e., pure water and dissolved monomer) (L)
V_d = Volume of monomer droplet phase (L)
V_p = Volume of particle phase (L)
V_pQ_0, V_pQ_1, V_pQ_2 = Zeroth, first and second moments of the molecular weight distribution (mol)
$V_pQ_0\overline{BN}_3$, $V_pQ_0\overline{BN}_4$ = Zeroth moments of the tri- and tetrafunctional branching frequency distributions (mol #/molecule)
V_T = Total reaction volume (i.e., volume of all reactor contents) (L)
V_w = Volume of pure water (L)
x = Overall monomer conversion
x_c = Conversion at the end of interval II in emulsion polymerization
α = Dimensionless group representing radical capture by particles
ε = Ratio of radical capture (radical absorption) between particles and micelles (k_{cp}/k_{cm})
θ = Mean residence time in a continuous reactor (min)
μ = Ratio of the rate constants for homogeneous and micellar nucleation (k_{h_o}/k_{cm})(dm^{-1})
ρ_p, ρ_{m_i} = Polymer and monomer densities (g/L)
$\phi^k_{m_i}$ = Volume fraction of monomer i in the phase k
ϕ^p_p = Volume fraction of polymer in the particle phase

1 Introduction

The use of mathematical models to simulate a process is common practice in almost all fields of science and engineering. Nowadays, with the increasing computational power of the personal computer, the application of models to predict real time information is becoming ever more practical. The polymer manufacturing industry is one example, where the use of powerful predictive models can aid in reducing product development time, improve process monitoring, control and optimization abilities, and inherently reduce process costs. With these common goals in mind, it is the purpose of this paper to present a mechanistic model that can be used to predict process behavior during the manufacture of nitrile-butadiene rubber (NBR), which will inherently assist in the improvement of process operability.

NBR is produced by polymerizing acrylonitrile (AN) and butadiene (Bd) monomers using a free radical mechanism in an emulsion system. The main indicators for product quality are the polymer molecular weight, degree of chain branching and level of bound AN in the copolymer. The average molecular weight usually ranges from 2.5×10^5 to 6×10^5 with varying degrees of polydispersity (e.g., 2 to 6) and branching. The level of bound AN can be varied (e.g., 15 to 50%) depending on a number of desired properties (e.g., oil/fuel resistance, tensile strength, heat resistance, resilience, flexibility). Other important product quality properties, due to their relation to molecular weight and chain branching, are Mooney viscosity and gel content. Hence, controlling Mooney and gel, in the rubber product, requires the direct control of molecular weight and chain branching within the reactor. Mooney can typically be thought of as a measure of molecular weight, where the units are arbitrary

and dependent on the test method used. Gel content on the other hand is not measured directly, but is instead related to stress relaxation which is an indicator of rubber plasticity.

Despite the long history of industrial production of NBR, little has been published in the open literature on the reaction engineering aspects of the process. Much of the existing literature focuses on the processing and resulting rubber properties. Perhaps, still to this day, the most comprehensive reports on rubber manufacture that cover both reaction engineering and processing are those of Bovey et al. (1) and Hofmann (2). Though these works provide great insight, much has been accomplished with respect to process modeling since these classic publications first appeared. Detailed reviews on mathematical techniques for emulsion polymerization systems can be found in de la Cal et al. (3), Dubé et al. (4), and Gao and Penlidis (5), while more specific applications of these techniques can be seen in Saldivar et al. (6), Casella et al. (7), Barclay et al. (8), and Alhamad et al. (9). The proposal of mathematical models specifically tailored for rubber production (styrene-butadiene (SBR) and NBR) that incorporate state-of-the-art process knowledge is limited to only a few publications, namely, the work of Broadhead et al. (10), Gugliotta et al. (11), Dubé et al. (12), Vega et al. (13), and Rodriguez et al. (14), where the latter three relate directly to NBR. Since the primary benefit from any model is the development of optimization and control strategies, potentially useful for industrial applications, it is no surprise that these particular models have been given considerable attention in the academic literature, whereby numerous control and optimization related activities have been proposed. For NBR in particular, strategies for controlling the molecular structure (i.e., copolymer composition and molecular weight), increasing polymer production, and reducing off-spec product during grade transitions have been proposed by Vega et al. (15) and Minari et al. (16–17).

The model developed in this paper considers micellar and homogeneous particle nucleation mechanisms, the latter being included due to the high water solubility of AN; radical propagation, termination, and reactions with impurities in both particle and aqueous phases; constant partition coefficients, chain transfer agent (CTA) and impurity phase partitioning; pseudo-kinetic rate constants for multiple monomers, CTA's and impurities; and radical desorption according to Asua et al. (18). Polymer and latex characteristics modeled are copolymer composition ($\bar{F}_{AN}$), average (mono-disperse) particle diameter ($\bar{d}_p$) and number of particles (N_p), number- and weight-average molecular weights ($\bar{M}_n$, $\bar{M}_w$) and tri- and tetra-functional branching frequencies ($\overline{BN}_3$, $\overline{BN}_4$). Though much of the modeling aspects shown in this paper were adapted from previous well established approaches (i.e., Broadhead et al. (10), Hamielec and McGregor (19), Mead and Poehlein (20), and Dubé et al. (12)), the contribution made in this paper was to bring these approaches together in unison and apply them to an NBR system, in parallel refining values of critical model parameters in order to obtain better predictions. More specifically, the particular approach used to determine the aqueous phase radical concentration in this paper has not yet been applied to an NBR system. Previous approaches used for rubber systems typically lump aqueous phase radical chain growth into an overall balance which ignores the possibility to selectively set the onset of radical capture as the radicals grow to their critical length. The approach considered in this paper conforms to current beliefs (e.g., see Thickett and Gilbert (21) for a recent review) that relatively water soluble radicals will propagate until they become active enough to enter newly formed micelles (i.e., micellar nucleation), enter existing particles, or instead simply remain in the aqueous phase until they reach a critical insoluble length whereby precipitation occurs (i.e., homogeneous nucleation).

2 Process Background and Model Development

2.1 Emulsion Copolymerization of AN/Bd

Nitrile rubber recipes are formulated based on the temperature at which polymerization takes place (hence, the terms 'cold' and 'hot' recipes), and on the desired final rubber properties. Cold recipes are those that use a redox radical initiation mechanism with temperatures in the range of 5 to 15°C. Hot recipes typically employ persulfate initiators in the range of 30 to 50°C. The final rubber properties are primarily governed by the ratio of AN to Bd and the amount of chain transfer agent used within the initial recipe. A typical example of both recipe types can be seen in Table 1.

Table 1. Typical nitrile rubber polymerization recipes (1–2)

Recipe Ingredient[a]	*Typical Chemicals*	*Cold NBR*	*Hot NBR*
Acrylonitrile		30–35	30–35
Butadiene		65–70	65–70
Water		170–200	170–200
Electrolyte	Na_2CO_3, K_2CO_3	0.3–0.5	0.3–0.5
Peroxide initiator	PMHP, DIBHP[b]	0.04–0.2	—
Metal ion	Iron chelate[c]	0.005–0.1	—
Reducing agent	SFS [d]	0.04–0.2	—
Persulfate initiator	KPS, SPS, APS[e]	—	—
Primary emulsifier[f]	Tamol, Daxad, SDS[g]	1.0–5.0	0.2–0.4
Secondary emulsifie [h]	Dresinate, Potassium Oleate, Emersol	0.1–5.0	1.0–5.0
Chain transfer agent	Mercaptan[i]	0.2–0.6	0.2–0.6
Temperature		5–15°C	30–50°C

[a] In parts per hundred monomer (pphm); [b] *para*-menthane (PMHP) or diisobutyl hydroperoxide (DIBHP); [c] e.g., chelated $FeSO_4 \cdot 7H_2O$; [d] Sodium formaldehyde sulfoxylate (SFS); [e] Potassium (KPS), sodium (SPS), or ammonium persulfate (APS); [f] Dispersing agent (condensed polyarylsulfonic acid salt); [g] Sodium dodecyl sulfate (SDS); [h] Fatty acid soap (e.g., stearic/palmitic acid); [i] e.g., tert-dodecyl mercaptan (t-DDM).

Table 2. Summary of pertinent literature on AN and Bd emulsion homo- and co-polymerization

Source	*System*	*Remarks*
Tazawa et al. (22)	AN	Batch experiments. Data on conversion, particle number and polymer yield.
Omi et al. (23)	AN	Semi-batch experiments and modeling. Data on polymer yield.
McCarthy et al. (24)	AN	Kinetic study under seeded conditions. Propagation rate constant estimation.
Nishida et al. (25)	AN	Plug-flow (tube) and continuous stirred reactor experiments. Data on conversion.
Morton et al. (26–27)	Bd	Propagation and chain transfer rate constants. Data on conversion.
Minhas (28)	Bd	Batch conversion data at different initiator and emulsifier levels.
Pallaske et al. (29)*	Bd	Data on conversion, diameter, and percent solids.
Weerts et al. (30–34)*	Bd	Data on conversion, particle size and number.
Deibert et al. (35–36)	Bd	Rate constants for propagation, termination, transfer to monomer.
Verdurmen et al. (37–42)	Bd	Transfer to monomer, termination, desorption rate coefficients.
Wall et al. (43)*	NBR	Data on conversion and bound AN.
Embree et al. (44)*	NBR	Data on bound AN and reactivity ratios.
Poddubny and Rabinerzon (45)*	NBR, SBR	Study of the influence of CTA on MWD.
Hofmann (2)*	NBR	Comprehensive review of NBR production.
Uraneck and Burleigh (46)*	NBR, SAN	Experimental data on conversion and effect of CTA on Mooney viscosity.
Burnett et al. (47–49)*	SBR	Rate constant information for crosslinking.
Vialle et al. (50)	NBR	Reactivity ratios
Guillot (51)	SAN	Modeling and experimental studies on partitioning.
Lin et al. (52)	SAN	Batch modeling and experimental validation.
Guyot (53), Guyot et al. (54)	SAN, NBR	Composition control, reactivity ratios.
Hoffman (55)	SAN	Batch modeling and experimental validation.
Omi et al. (56)	SAN	Semi-batch modeling and experimental data on yield.
Shvetsov (57)	NBR	Batch reactor experimental data on N_p, conversion, PSD.
Filho et al. (58)	SBR	Batch modeling and experimental validation.

*Sources found most useful to the current investigation for experimental data and reaction rate constants.

For a detailed description of the functionality of each ingredient refer to Hofmann (2).

Literature relating to the emulsion polymerization of AN and Bd separately as homopolymers and together as a copolymer is quite limited. However, there are a few sources that address the rate constants for propagation, transfer to monomer, transfer to chain transfer agent, and termination. A detailed listing of past work on both mechanistic and kinetic aspects of emulsion polymerization of AN and Bd is provided in Table 2. Of these past studies, some are relevant in determining a starting database of kinetic parameters, as well as providing representative reaction data sources for emulsion homo- and co-polymerization, which will subsequently be used for model testing and validation (see section 3). Table 3 provides such a listing of potential parameter values for establishing an initial database. Further discussion on the parameters used in the model of this paper is provided in section 2.8.

2.2 NBR Reactor Model Development

The model used in this paper is based on the model presented by Dubé et al. (12), where an extension of the material balances was made to account for the continuous regime. Details on the mathematical model equations are given in Appendix A. Several explanatory remarks will be made in the following subsections. Throughout the paper, if symbols are not defined upon first use, they are cited in the nomenclature section.

2.3 Reaction Kinetics

The reaction rate of each species in each phase of the reaction medium can be defined assuming a first order reaction with respect to each reactant. Based on the mechanism shown in Table 4, a general rate expression for each reaction can be written as follows:

$$R_{i_k} = k_i[i]_k[j]_k \tag{1}$$

where $[i]_k$ and $[j]_k$ correspond to the concentration of reactants i and j in phase k, and k_i represents the reaction rate constant given as a function of temperature according to an Arrhenius expression.

The rate of polymerization (monomer consumption) can be expressed for the reaction of monomer j with a radical ending in monomer i using the following equation:

$$R_{p_{j_k}} = [R]_k[M]_k f_{j_k} \sum_{i}^{N_m} (k_{p_{ij_k}} \phi_{i_k}^{\cdot}) \tag{2}$$

Table 3. Literature values of AN and Bd propagation, termination, and transfer rate constants (A = AN, B = Bd).

Process	*Parameter*	*Expression*	*Value*[a]	*Source*
Propagation	$k_{p_{AA}}$	$1.8 \times 10^9 \exp(-4100/RT)$	3.04×10^6	(59)[b]
	$k_{p_{AA}}$	$6.282 \times 10^9 \exp(-7278.38/RT)$[c]	7.5×10^4	(60)
	$k_{p_{AA}}$	—	1.2×10^6[d]	(61)
	$k_{p_{AA}}$	—	1.8×10^4–7.2×10^4	(24)
	$k_{p_{BB}}$	$7.2 \times 10^9 \exp(-9300/RT)$	5.7×10^3	(27)
	$k_{p_{BB}}$	$4.83 \times 10^9 \exp(-8531/RT)$	1.22×10^4	(35)[e]
	$k_{p_{BB}}$	—	1.2×10^4	(30)
	$k_{p_{BB}}$	—	$1.92 \times 10^4 \pm 16\%$	(37)
Termination	$k_{t_{AA}}$	$1.98 \times 10^{12} \exp(-5400/RT)$	4.4×10^{11}	(59)
	$k_{t_{AA}}$	$1.603 \times 10^{16} \exp(-5400/RT)$ [f]	2.3×10^9[g]–3.6×10^{12}[f]	(62)
	$k_{t_{BB}}$	$6.78 \times 10^{11} \exp(-1412.76/RT)$	8.02×10^{10}	(35)[e]
	$k_{t_{BB}}$	—	4.2×10^{11}	(37)
Transfer to monomer	$k_{fm_{AA}}$	$(0.3 \times 10^{-4}$–$1.0 \times 10^{-4}) \times k_{p_{AA}}$	2.2–7.5[h]	(63)
	$k_{fm_{AA}}$	$6.545 \times 10^7 \exp(-10972.37/RT)$	2.48	(12)
	$k_{fm_{BB}}$	$5.278 \times 10^8 \exp(-12993.98/RT)$	0.86	(12)
	$k_{fm_{BB}}$	$2.532 \times 10^8 \exp(-10213.18/RT)$	50.5	(35) [e]
	$k_{fm_{BB}}$	—	6	(30)
	$k_{fm_{BB}}$	—	0.6–6	(37)
Transfer to CTA	k_{fcta_A}	$0.73 \times k_{p_{AA}}$	5.5×10^4	(63)
	k_{fcta_B}	$3.06 \times 10^8 \exp(-6400/RT)$	1.936×10^4	(27)

[a]Numerical value at 50°C; [b]From AN solution polymerization; [c]Estimated in conjunction with styrene as a comonomer; [d]Reported at 40°C for AN solution polymerization; [e]From Bd solution polymerization in chlorobenzene; [f]Aqueous phase estimate; [g]Particle phase estimate; [h]Using $k_{p_{AA}}$ of Garcia-Rubio et al. (60) at 50°C (see c).

where $[R^{\cdot}]_k$ and $[M]_k$ represent the total concentration of radicals and monomer in phase k; f_{j_k} and $\phi^{\cdot}_{i_k}$ describe monomer and radical mole fractions for monomer j and radical i; $k_{p_{ij_k}}$ corresponds to the propagation rate constant between monomer j and radicals ending in monomer i for phase k; N_m represents the total number of monomers in the system. Radicals are assumed only to be active in particle and aqueous phases.

Pseudo-rate constants provide a convenient way of handling multicomponent systems. They allow the reaction kinetics to be described based on the fraction of free-radicals, monomer, polymer, or impurity present in the reactor. A few examples of pseudo-rate constants are provided in Equations 3–6. To determine the pseudo-propagation rate constant, information from individual rate constants for each monomer (given by an Arrhenius expression), cross-propagation rate constants (described through reactivity ratios), and monomer and radical mole fractions is summarized in the overall propagation rate constant given by the following expression:

$$k_{p_k} = \sum_{i}^{N_m} \sum_{j}^{N_m} k_{p_{ij_k}} \phi^{\cdot}_{i_k} f_{j_k} \tag{3}$$

Note that the values of $\phi^{\cdot}_{i_k}$ and f_{j_k} will differ from particle to aqueous phases. Therefore the pseudo-rate constant in each of these phases will differ.

Rate constants for transfer to polymer or for reaction with double bonds along polymer chains differ from those of monomer-radical reactions. Since these reactions involve a radical and a polymer chain, the rate constant now employs the polymer mole fraction as opposed to the monomer mole fraction (f_j).The polymer mole fraction can be thought of as the cumulative copolymer composition ($\bar{F}_j$). For transfer to polymer, the pseudo-rate constant can be expressed as:

$$k_{fp_k} = \sum_{i}^{N_m} \sum_{j}^{N_m} k_{fp_{ij_k}} \phi^{\cdot}_{i_k} \bar{F}_{j_k} \tag{4}$$

For free-radical reactions with species such as impurities or CTA, the pseudo-rate constants can be expressed in a similar manner to monomer-related reactions, the only difference now being in the use of the mole fraction $f_{x_{j_k}}$ to describe the contribution from each ingredient. In general, the rate expression can be defined as:

$$k_{fx_k} = \sum_{i}^{N_m} \sum_{j}^{N_x} k_{fx_{ij_k}} \phi^{\cdot}_{i_k} f_{x_{j_k}} \tag{5}$$

where N_x represents the number of impurities or CTAs in the reactor (depending on which is considered). Note that if there is no distinction/preference with respect to radical

Table 4. Reactions and other events

Mechanism	*Reaction/Event*
Redox decomposition	$S_2O_8^{2-} + Fe^{2+} \xrightarrow{k_1} SO_4^{-\cdot} + Fe^{3+} + SO_4^{2-}$
	$Fe^{3+} + SFS \xrightarrow{k_2} Fe^{2+} + SFS^{+}$
Thermal decomposition	$S_2O_8^{2-} \xrightarrow{k_d} 2SO_4^{-\cdot}$
Radical initiation	$SO_4^{-\cdot} + M_j \xrightarrow{k'_{p_{ja}}} R_{1,j}^{\cdot}$
Propagation	$R_{n,i}^{\cdot} + M_j \xrightarrow{k_{p_{ij}}} R_{n+1,j}^{\cdot}$
Termination	$R_{n,i}^{\cdot} + R_{m,j}^{\cdot} \xrightarrow{k_t} P_{(m+n)}$ or $P_n + P_m$
Transfer to monomer	$R_{n,i}^{\cdot} + M_j \xrightarrow{k_{fm_{ij}}} P_{n,i} + M_j^{\cdot}$
Transfer to polymer	$R_{n,i}^{\cdot} + P_{m,j} \xrightarrow{k_{fp_{ij}}} P_{n,i} + R_{m,j}^{\cdot}$
Transfer to CTA	$R_{n,i}^{\cdot} + (CTA)_j \xrightarrow{k_{fcta_{ij}}} P_{n,i} + CTA_j^{\cdot}$
Reaction with internal double bonds	$R_{n,i}^{\cdot} + P_m^{i=} \xrightarrow{k^{**}_{p_{ij}}} R_{n+m,i}^{\cdot}$
Reaction with terminal double bonds	$R_{n,i}^{\cdot} + P_m^{t=} \xrightarrow{k^{*}_{p_{ij}}} R_{n+m,i}^{\cdot}$
Reaction with water-soluble impurities	$R_{n,i}^{\cdot} + WSI_j \xrightarrow{k_{fwsi_{ij}}} P_i$
Reaction with monomer-soluble impurities	$R_{n,i}^{\cdot} + MSI_j \xrightarrow{k_{fmsi_{ij}}} P_i$
Micellar nucleation	$R_{n,i}^{\cdot} + \text{Micelle} \xrightarrow{k_{cm}} \text{Particle}$
Homogeneous nucleation	$R_{j_{cr},i}^{\cdot} + M_j \xrightarrow{k_h} \text{Particle}$
Capture of radical by particle	$R_{n,i_a}^{\cdot} \xrightarrow{k_{cp}} R_{n,i_p}^{\cdot}$
Desorption of radical from particle	$R_{1,i_p}^{\cdot} \xrightarrow{k_{des}} R_{1,i_a}^{\cdot}$

reactivity between each impurity or CTA, then Equation 5 can be simplified to:

$$k_{fx_k} = \sum_{i}^{N_m} k_{fx_{i_k}} \phi_{i_k}^{\cdot} \tag{6}$$

where the rate constant is now only a function of radical type.

2.4 Species Partitioning

Accurate monomer partitioning models are of great importance in an emulsion system, since they enable the determination of the rate of polymerization, and hence copolymer composition, conversion, and molecular weights. In a multiphase system (particle, aqueous, and droplet phases), monomer partitions between each phase depending on its relative phase solubility. Since the rate of monomer mass transfer is typically much higher than the rate of polymerization, a thermodynamic equilibrium of the monomer between each phase exists while each of the three phases are present. Considering these aspects, much of the theoretical work on monomer partitioning has been on establishing accurate thermodynamic models to describe the concentration of monomer in each phase (64–67).

The approach used in this paper employs what is commonly known as the partition coefficient method. In this approach, the mole fraction of monomer (or concentration) in each respective phase is defined in terms of partition coefficients, which are assumed to remain constant over the course of polymerization (or at least until the respective phases disappear). More specifically, our approach uses one partition coefficient to describe the distribution of monomer between the particle and aqueous phases; a balance on monomer in the aqueous phase where the concentration is assumed to remain at the solubility limit until the droplet phase disappears, after which monomer is envisioned to transfer from the aqueous phase into the particle phase at a rate proportional to the rate of monomer consumption.

The moles of monomer in the droplet phase can be determined by taking the difference of the moles in aqueous and particle phases from the total moles of monomer in the system. Once the droplet phase is consumed (i.e., stage 3 of emulsion polymerization), the partition coefficient is no longer used, as the aqueous and particle phases are no longer at equilibrium; instead, the number of moles of monomer in the particle phase is determined by taking the difference between the total moles in the system and the moles in the aqueous phase, which are both states in the model.

2.5 Particle Nucleation

The overall number of particles nucleated can be determined by typically considering micellar and homogeneous nucleation mechanisms, following Hamielec et al. (68) and Dubé et al. (4). In our development, only a fraction of the radicals initiated are considered to be captured by micelles, while the remaining are captured by particles or undergo homogeneous nucleation.

Micellar nucleation occurs when a radical is captured by a micelle forming a polymer particle. The process of radical capture (or absorption) has been described by essentially equivalent radical collision or diffusion theories (see, for instance, Gao and Penlidis (5)). In this paper, collision theory has been adopted and an expression based on a variant of the collision theory equations can be written as:

$$R_{mic} = R_{des}^{mic} + \left(\frac{k_{cm}[R^{\cdot}]_a^{mic}}{r_{mic}}\right) N_A \tag{7}$$

where R_{mic} is the rate of micellar nucleation, R_{des}^{mic} accounts for the rate at which desorbed radicals are recaptured by micelles, and the second portion of the equation accounts for the usual capture of radicals formed from initiator, where

k_{cm} is the "rate constant" for radical capture by micelles, $[R^{\cdot}]_a^{mic}$ represents the concentration of radicals in the aqueous phase that are capable of being captured by micelles, and r_{mic} is the approximate micelle radius (i.e., micelles are assumed to be monodisperse with a constant radius).

Homogeneous nucleation occurs when radicals grow in the aqueous phase to a critical chain length (j_{cr}) at which they become insoluble and precipitate forming polymer particles. The particle formation process considered in this paper uses HUFT (Hansen-Ugelstad-Fitch-Tsai) theory with the necessary modifications to include radical desorption, where the aqueous phase radical concentration is determined by performing a population balance on radicals of chain length less than their critical value. The resulting rate expression for homogeneous nucleation can be formulated as:

$$R_{hom} = k_h [R^{\cdot}]_a^{hom} V_a N_A \tag{8}$$

where the extent of homogeneous nucleation is dependent on the "rate constant" k_h and the radical concentration in the aqueous phase that could potentially contribute to homogeneous nucleation ($[R^{\cdot}]_a^{hom}$). k_h can be formulated as:

$$k_h = \begin{cases} k_{h_o}\left(1 - \frac{LA_p}{4V_a}\right) & \text{if } LA_p < 4V_a \\ 0 & \text{otherwise} \end{cases} \tag{9}$$

where L represents the average distance a radical travels before precipitation; k_{h_o} corresponds to the initial homogeneous "rate constant" value at zero conversion; V_a is the aqueous phase volume (i.e., water and dissolved monomer); and A_p is the total particle surface area.

For an AN/Bd system, previous modeling efforts (12) assumed that radicals of chain length greater than $k = j_{cr}/2$ are capturable, Bd radicals precipitate at a length of $j_{cr}/2$, and AN radicals precipitate at j_{cr} unless a Bd unit is added, at which point the radical immediately precipitates to form a particle. Therefore, by applying the quasi-steady-state hypothesis (QSSH) to population balances for radicals of chain length k, expressions for $[R^{\cdot}]_a^{mic}$ and $[R^{\cdot}]_a^{hom}$ can be formulated. Considering all radicals of chain length greater than $k = j_{cr}/2$, these expressions can be written as follows:

$$[R^{\cdot}]_a^{mic} = \sum_{k=j_{cr}/2+1}^{j_{cr}-1} [R_k^{\cdot}]_a \left(\frac{A_m}{A_m + \varepsilon A_p}\right) + [R_{j_{cr}}^{\cdot}]_a \left(\frac{A_m}{A_m + \varepsilon A_p + \mu H}\right) \tag{10}$$

$$[R^{\cdot}]_a^{hom} = [R_{j_{cr}}^{\cdot}]_a \left(\frac{\mu H}{A_m + \varepsilon A_p + \mu H}\right) \tag{11}$$

The first portion of Equation (10) represents the concentration of radicals capturable up to a chain length of $j_{cr} - 1$, whereas the second portion accounts for the concentration of radicals that can be captured given the chance that they could also undergo homogeneous nucleation at j_{cr}. Equation (11), on the other hand, represents the total radical concentration that can undergo homogeneous nucleation at j_{cr}. Some other important variables and parameters appearing in these equations are the total free micellar area (A_m), the ratio of radical capture between particles and micelles ($\varepsilon = k_{cp}/k_{cm}$), the ratio of radicals formed by homogeneous to micellar nucleation ($\mu = k_{h_o}/k_{cm}$), and the fraction of homogeneous nucleation occurring in the system (H). Expressions for these variables are given in Appendix A, whereas values of all parameters used are cited in Appendix B.

2.6 Average Number of Radicals per Particle

Over the years, there have been many different variations for formulating and solving both steady-state and transient expressions for the average number of radicals per particle ($\bar{n}$). The approach that is used in this paper follows that of Huo et al. (69), which is based on a steady-state approximation and accounts for monomer impurities. This expression is as follows:

$$\bar{n} = \frac{\alpha}{p + \frac{2\alpha}{p+1+\frac{2\alpha}{p+2+\cdots}}} \tag{12}$$

where α and p are dimensionless terms (given in Appendix A) that represent radical "gain" via radical capture by particles and radical "loss" through radical desorption from the particles or radical consumption from impurities. As mentioned by Dubé et al. (4), Equation 12 was found to require approximately 10 levels of fractions to obtain adequate convergence in $\bar{n}$ and this was deemed sufficient enough to describe the kinetics of an NBR system, while providing a desirable level of computational efficiency.

2.7 Molecular Weight Averages/Branching Frequencies

The approach taken in this paper to develop equations to describe average molecular weight and chain branching frequencies considers transfer reactions to small molecules (i.e., monomer, CTA, and monomer-soluble impurities), termination reactions, transfer to polymer, terminal double bond polymerization and internal double bond polymerization, and employs the method of moments.

Expressions defining number- and weight-average molecular weights ($\bar{M}_n$, $\bar{M}_w$) and tri- and tetra-functional branching frequencies ($\overline{BN}_3$, $\overline{BN}_4$) can be defined as follows:

$$\bar{M}_n = M_{\text{eff}} \frac{V_p Q_1}{V_p Q_0} \tag{13}$$

$$\bar{M}_w = M_{\text{eff}} \frac{V_p Q_2}{V_p Q_1} \tag{14}$$

$$\overline{BN}_3 = \frac{V_p Q_0 \overline{BN}_3}{V_p Q_0} \tag{15}$$

$$\overline{BN}_4 = \frac{V_p Q_0 \overline{BN}_4}{V_p Q_0} \tag{16}$$

where M_{eff} is the effective monomer molecular weight and is defined by weighing the individual monomer molecular weights by the respective cumulative copolymer compositions; $V_p Q_0$, $V_p Q_1$, $V_p Q_2$ are the first three moments of the molecular weight distribution (MWD) defined on a mole basis and are states of the model, with V_p representing the particle phase volume; and finally, $V_p Q_0 \overline{BN}_3$ and $V_p Q_0 \overline{BN}_4$ are zeroth moments of the tri- and tetra-functional branching distributions, again states of the model. Each of the aforementioned states are defined through differential equations (refer to Appendix A for further details).

2.8 Model Parameter Database

For the most part, physico-chemical characteristics, kinetic rate constants and other parameters were obtained from literature sources on AN, Bd, NBR, and SBR. Dubé et al. (12) provide a detailed listing of the parameters used in their NBR model, and many of these parameters were used in the model of this paper (at least as a starting point). Inevitably, adjustments were made to certain parameters in order to obtain a better fit of the model to literature data. A detailed discussion was given by Wong (70), Gugliotta et al. (11) and Vega et al. (13) on parameter adjustment for the cases of SBR and NBR, and following the advice given, a similar procedure was adopted in order to obtain reasonable estimates that were in the range of reported literature findings. A detailed listing of the final parameters arrived at in this paper is provided in Appendix B. The following discussion provides a comparison of some of the more important kinetic parameters used in previous modeling efforts, and justification for the parameters used in this paper.

Comparing the parameters used in the models of Dubé et al. (12) and Vega et al. (13) can provide a relative range of values from which further refinement can be made. Table 5 compares the rate constants reported in the previously mentioned papers and also cites the original literature source of the kinetic expressions. A few discrepancies in the reported values can be readily seen, more specifically in the values of $k_{p_{AA}}$, $k_{fm_{AA}}$, and $k_{fp_{AA}}$.

The homopropagation rate constant for acrylonitrile ($k_{p_{AA}}$) used by Vega et al. (13) (3.98×10^5 L/mol/min at 10°C) is quite high compared to that used by Dubé et al. (12) (1.51×10^4 L/mol/min at 10°C). Dubé et al. (12) used the expression given by Garcia-Rubio et al. (60) who previously demonstrated their value to be adequate for styrene-acrylonitrile (SAN) bulk copolymerization. Furthermore, McCarthy et al. (24) performed experiments on AN under seeded conditions and suggested an approximate range for the propagation rate constant of 1.8×10^4 to 7.2×10^4 L/mol/min at 50°C, which is in agreement with the value given by the Arrhenius expression used by Dubé et al. (12) (7.5×10^4 L/mol/min at 50°C). From the perspective of parameter sensitivity on the overall conversion, Dubé et al. (12) suggested a parameter range of 1.5×10^4 to 1.5×10^5 at 10°C. Based on the experimental findings mentioned above, the lower value used by Dubé et al. (12) is believed to be a more reasonable choice than the higher value used by Vega et al. (13).

Table 5. Comparison of NBR kinetic rate constants

	Dubé et al. (12)		*Vega et al. (13)*	
Parameter	*Value*[a]	*Source*	*Value*[b]	*Source*
$k_{p_{AA}}$	1.51×10^4	(60)	3.98×10^5	(63)
$k_{p_{BB}}$	4.77×10^2	(27)	5.30×10^2	(63)
$r_A = k_{p_{AA}}/k_{p_{AB}}$	0.05	(63)	0.03	(63)
$r_B = k_{p_{BB}}/k_{p_{BA}}$	0.35	(63)	0.30	(63)
$k_{fm_{AA}}$	0.22	(12)	2.00	(63)
$k_{fm_{BB}}$	0.049	(12)	0.01	(70–71)
$k_{fm_{BA}}$	0	(12)	$k_{fm_{AA}}$	(13)
$k_{fm_{AB}}$	0	(12)	$k_{fm_{BB}}$	(13)
$k_{fp_{AA}}$	0	(12)	1.10	(63)
$k_{fp_{BB}}$	0.09	(71)	0.055	(70)
$k_{fp_{BA}}$	0	(12)	$k_{fp_{AA}}$	(13)
$k_{fp_{AB}}$	$k_{fp_{BB}}$	(12)	$k_{fp_{BB}}$	(13)
$k^{**}_{p_{AA}}$	0	(12)	0	(13)
$k^{**}_{p_{BB}}$	9.68×10^{-3}	(48)	9.56×10^{-3}	(48)
$k^{**}_{p_{BA}}$	$k^{**}_{p_{AA}}$	(12)	$k^{**}_{p_{AA}}$	(13)
$k^{**}_{p_{AB}}$	$k^{**}_{p_{BB}}$	(12)	$k^{**}_{p_{BB}}$	(13)
$k_{t_{AAa}}$	1.09×10^{12}[c]	(62)	—[d]	—
k_{fcta_A}	3.02×10^5	(12)	1.28×10^5	(63)
k_{fcta_B}	1.71×10^2	(12)	2.41×10^2	(13)

[a]Evaluated at 10°C from an Arrhenius expression; [b]Given at 10°C, no Arrhenius expression reported; [c]The overall k_{t_a} (i.e., overall aqueous phase termination) is assumed to be equal to $k_{t_{AAa}}$; [d]No estimate reported.

As a result of the relatively high AN propagation rate constant, the rate constant used by Vega et al. (13) for transfer to AN monomer from a radical ending in AN ($k_{fm_{AA}}$) is also quite high. This can be seen from the transfer constant ($C_{fm} = k_{fm_{AA}}/k_{p_{AA}}$) used to obtain the transfer rate constant estimate. Vega et al. (13) also assumed that transfer to monomer AN or Bd is independent of the radical type that is transferring its activity (i.e., $k_{fm_{AA}} = k_{fm_{BA}}$ and $k_{fm_{BB}} = k_{fm_{AB}}$). On the contrary, Dubé et al. (12) assumed that radicals only transferred to monomer of the same type (i.e., $k_{fm_{BA}} = 0$ and $k_{fm_{AB}} = 0$). This assumption was made to avoid introducing further uncertainly into the model. Performing simulations considering the assumption used by Vega et al. (13) and the k_{fm} parameters of Dubé et al. (12), revealed an insignificant change in the overall conversion. The assumption made by Dubé et al. (12) was thus followed in this paper.

Also evident in Table 5 are differences in the rate constants for transfer to AN in the dead polymer ($k_{fp_{AA}}$, $k_{fp_{BA}}$). Dubé et al. (12) assumed that it would be more likely that transfer to polymer only occur with Bd units in

the polymer (i.e., $k_{fp_{BB}}$, $k_{fp_{AB}}$). This assumption was based on the findings of Garcia-Rubio et al. (60), who showed that with an SAN system only linear chains are formed. Thus, any branching that occurs is most likely due to the Bd contribution.

Another difference between the parameters given in Table 5 is the values of the reactivity ratios used. The polymer handbook (63) lists a number of slightly different estimates for r_A and r_B, which all predict slightly different azeotropic compositions (i.e., $F_{AN} = f_{AN}$). For the particular ratios used by Dubé et al. (12) and Vega et al. (13), a copolymer composition curve can be constructed as seen from Figure 1. Comparing the azeotropic composition from each set of ratios reveals only minor differences. As an added feature, Figure 1 also includes experimental data from Embree et al. (44).

The rate constants for transfer to CTA used by Dubé et al. (12) and Vega et al. (13) are of the same order of magnitude. Simulation studies by Vega et al. (13) show that the transfer constant (C_{fcta}) for t-dodecyl mercaptan with a value of 0.32 at 10°C adequately predicts number- and weight-average molecular weights when compared to experimental data. On the other hand, Uraneck and Burleigh (46) state that for an NBR system, initially with a AN/Bd ratio of 30/70, the transfer constant should be around 1.1. Taking into consideration this approximate range for C_{fcta}, appropriate adjustments were made in order that C_{fcta} was close to this range while providing a reasonable fit to the experimental data of Vega et al. (13). More specifically, the approach taken to establish k_{fcta_B}, was to lower the value given by Morton et al. (27) until reasonable predictions were obtained, while for k_{fcta_A}, an estimate was obtained by starting with the propagation rate constant $k_{p_{AA}}$ and adjusting it accordingly until a reasonably good fit was obtained.

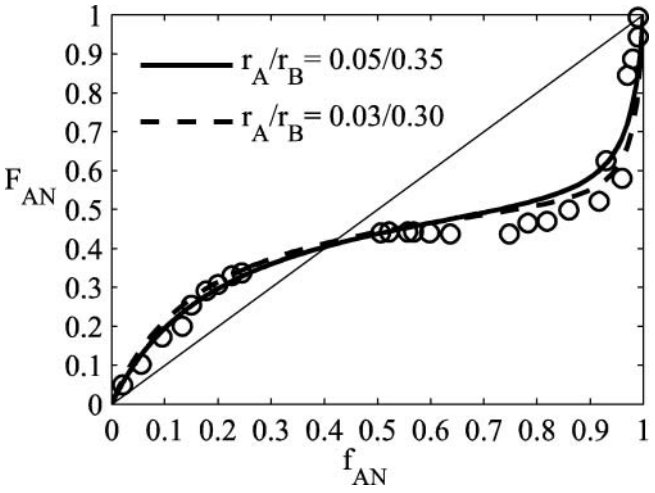

Fig. 1. Instantaneous copolymer composition of AN as a function of the feed mole fraction of AN (Mayo-Lewis Equation).

The influence of radical desorption in an NBR system was found to be minimal. Increasing the value of $k_{fm_{AA}}$ ten-fold according to the value used by Vega et al. (13), made little difference on the prediction profiles. Therefore, desorption was excluded from all model simulations shown in this paper.

Table 6. NBR and Bd emulsion polymerization batch reactor recipes

	NBR			*Bd*	
Ingredient[a]	*Recipe 1 (12)*	*Recipe 2 (12)*	*Recipe 3 (13)*	*Recipe 4 (72)*	*Recipe 5 (29)*
Acrylonitrile	27.5	32	31	—	—
Butadiene	72.5	68	69	100	100
Water	180	180	180	230	168
KPS	0.25	—	—	—	0.328
SPS	—	—	—	0.7	—
PMHP	—	0.223	0.2	—	—
$FeSO_2 \cdot H_2O$	—	0.0056	0.005	—	—
SFS	—	0.12	0.1	—	—
SDS	—	—	—	7.6	—
Potassium Oleate	—	—	—	—	0.87
Dresinate	—	1.25	1.25	—	—
Emersol	1.16	—	—	—	—
Tamol	—	2.85	2.75	—	—
Daxad	2.85	—	—	—	—
t-Dodecyl Mercaptan	0.6	0.42	0.375	0.7	0.7
$[E]_o$(mol/L)	0.0317	0.0373	0.0367	0.1122	0.0160
$[I]_o$(mol/L)	0.0046	0.0065	0.0058	0.0128	0.0072
Temperature(°C)	40	10	10	40	68

[a]In parts per hundred monomer (pphm).

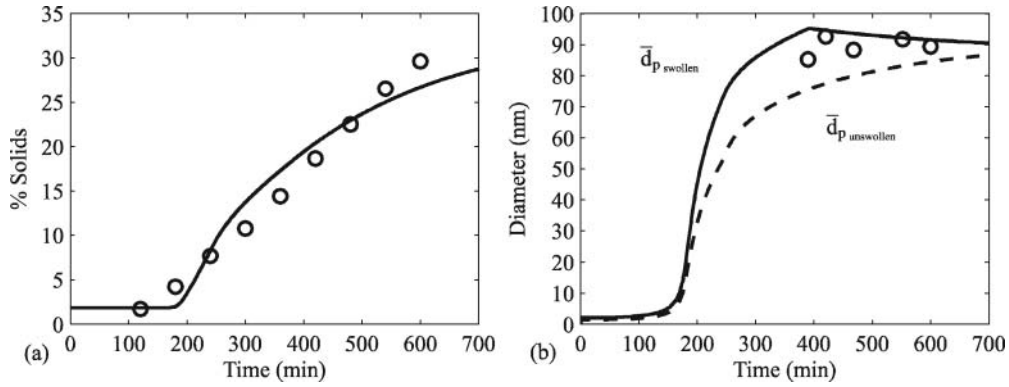

Fig. 2. NBR batch reactor simulation and comparison to pilot plant data (12) (recipe 1 in Table 6) for percent solids (a) and average particle diameter (b).

3 Results and Discussion

3.1 Model Validation and Literature Data Comparison

In order to provide an idea of the validity of the model, comparisons are made to available process data found in the literature. The only available literature sources for such data are the previous modeling studies of Dubé et al. (12) and Vega et al. (13). Due to the limited availability of NBR data, comparisons are also made to polymerization of Bd alone, where the model was reduced to describe emulsion homopolymerization. Weerts (72) provided an excellent source of information on the emulsion homopolymerization of Bd under laboratory conditions, while Pallaske et al. (29) provided information on a larger pilot plant scale. A listing of the recipes used for model validation is provided in Table 6.

3.2 NBR Batch Reactor Comparisons

A comparison between the model and pilot plant data for recipe 1 in Table 6 is shown in Figure 2. The agreement between percent solids data and model prediction is quite satisfactory (see Fig. 2a). From the percent solids data it is quite clear that an induction period is present at the beginning of the reaction, as a result of water soluble impurities (WSI), which are taken into account in the model.

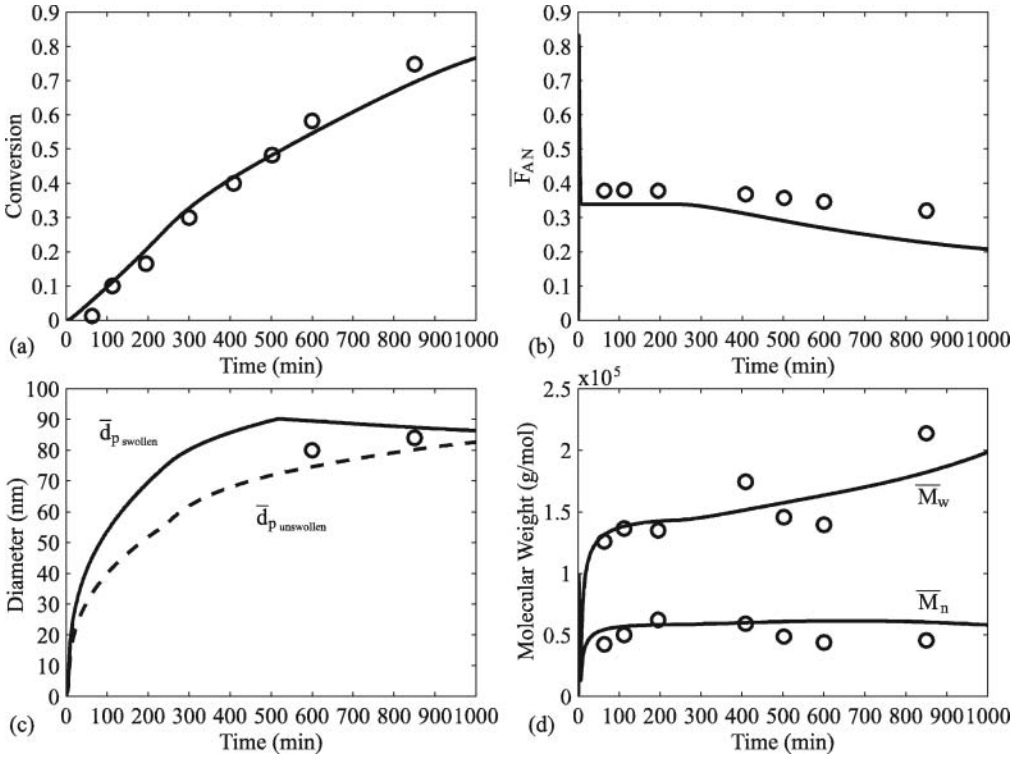

Fig. 3. NBR batch reactor simulation and comparison to the industrial data of Vega et al. (13) for conversion (a), cumulative copolymer composition (b), average particle diameter (c) and molecular weight averages (d).

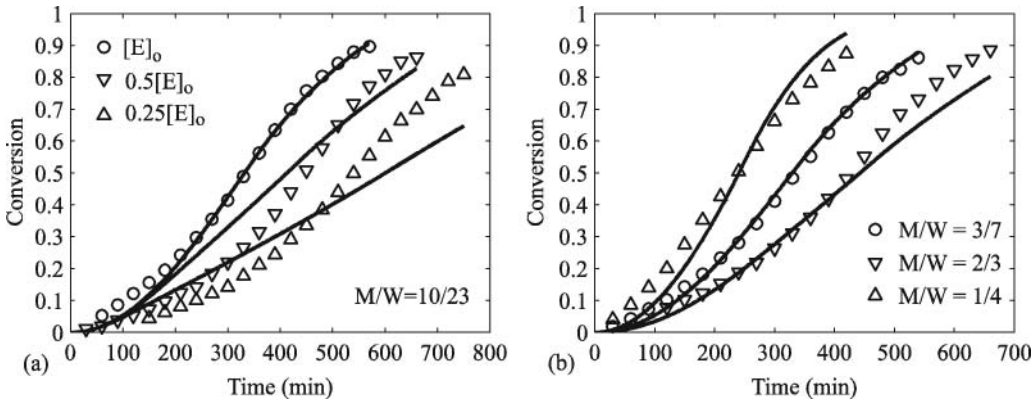

Fig. 4. Bd emulsion polymerization batch reactor simulation and comparison to experimental data of Weerts (72) for conversion with several emulsifier concentrations ($[E]_o$) (a) and monomer to water ratios (M/W) (b).

In fact, the present model takes into account both water soluble and monomer soluble impurities (MSI), and is in agreement with respect to impurity effects with the work of Penlidis et al. (73) and Huo et al. (69). Furthermore, the agreement between limited average particle diameter data and model predictions, shown in Figure 2b, is also satisfactory.

The experimental information provided by Vega et al. (13) (recipe 3 in Table 6) was significantly more comprehensive than that reported by Dubé et al. (12). Data on conversion, copolymer composition, particle diameter and molecular weight were reported. Due to the industrial nature of the data, the presence of impurities was certain. Vega et al. (13) reported the presence of oxygen and vinylacetylene as impurities. Simulations with the present model are shown in Figure 3. Again, the overall picture is quite satisfactory.

3.3 Bd Batch Reactor Comparisons

Using recipe 4 (of Table 6) from Weerts (72), simulation profiles for Bd emulsion homopolymerization were compared to experimental data considering several different emulsifier levels and monomer to water ratios. The purpose in performing such comparisons was to demonstrate the model's predictive ability and sensitivity to changes in the recipe. Figure 4 reveals the influence of both emulsifier concentration and monomer to water ratio for three different experiments. Initial parameter adjustments of ε were made to fit the base emulsifier level (i.e., $[E]_o = 0.1122$ mol/L) in Figure 4a, while all other parameters were unaltered from the values given in the established database (see Appendix B). Notice that in both Figure 4a and 4b profiles for the base emulsifier and monomer to water ratio (i.e., M/W = 3/7) provide a very good fit to the experimental data for the nucleation parameter $\varepsilon = 0.4839$; however, as the emulsifier and monomer to water ratio levels are varied model predictions appear to degrade. This discrepancy between data and model predictions when the emulsifier concentration is altered is not unexpected, as both emulsifier concentration and the value of parameter ε influence the extent of micellar nucleation and hence the number of particles generated and the resulting rate of polymerization.

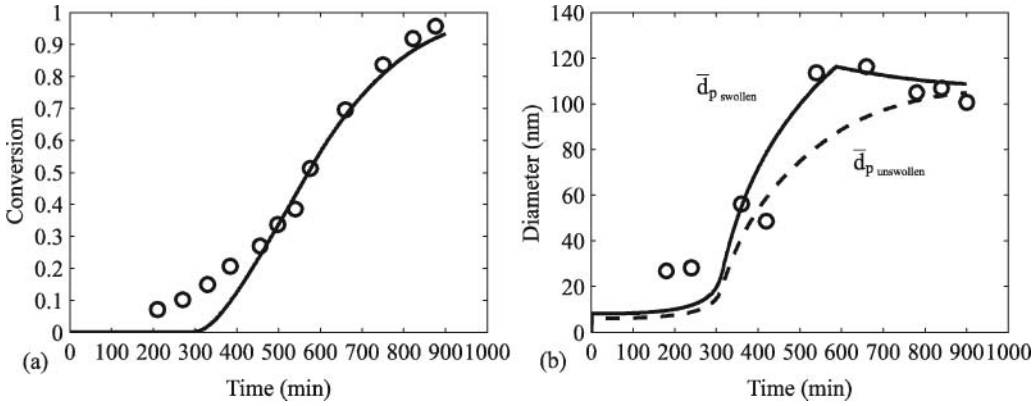

Fig. 5. Bd emulsion polymerization batch reactor simulation and comparison to data of Pallaske et al. (29) for conversion (a) and average particle diameter (b).

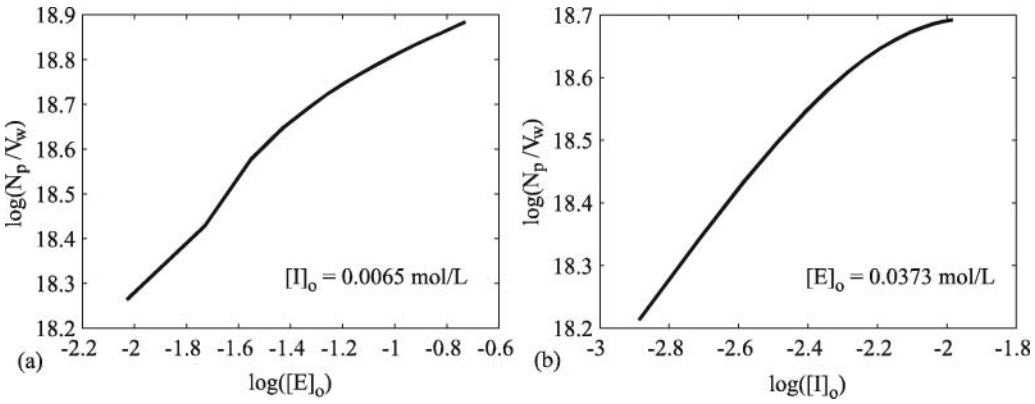

Fig. 6. NBR batch reactor simulation of particle number (N_p) for different reactor concentrations of emulsifier ($[E]_o$) (a), and initiator ($[I]_o$) (b).

Finally, Figure 5 provides a model comparison to the data of Pallaske et al. (29) (recipe 5 of Table 6) for conversion and particle diameter. Figure 5a reveals good agreement between model and conversion data beyond 400 min, while prior to this point a clear discrepancy is present.

Similarly, particle diameter is predicted satisfactorily beyond 350–400 min and not so well early on. This behavior may suggest the presence of other, unaccounted for, impurities, most likely of the monomer soluble type. Given that this information is not available, the results of Figure 5 are deemed satisfactory overall.

3.4 Model Applications

In the previous section, it was demonstrated that the model was able to adequately predict the trends shown with four different batch data sets for NBR and Bd. In this section, we provide further examples of the model's uses, and how it can shed light on several important aspects of process operation, including the effects of modifying the emulsifier or initiator concentration in batch and continuous reactors; the effect of the start-up procedure for a continuous reactor; the evolution of reactor properties in a reactor train; how one may introduce recipe ingredients into downstream reactors in order to control polymer properties; how one can redistribute the monomer feed to the reactor train, in addition to feeding ingredients to downstream reactors, with the ultimate goal of increasing polymer productivity. These case studies are now addressed in turn.

3.5 Influence of Emulsifier and Initiator Concentration on Particle Nucleation

Having a good understanding of the influence of emulsifier and initiator concentration on particle nucleation can allow one to efficiently formulate product recipes so that the optimal number of particles is obtained. In order to assess the influence of emulsifier and initiator concentration and to compare this influence with that seen in the classic studies of Smith and Ewart (74), the model was used to simulate several cases based now on recipe 2 of Table 6. Figure 6 displays results for a batch reactor for a concentration range of 9.325×10^{-3}–1.865×10^{-1} mol/L for emulsifier and 1.3×10^{-3}–1.04×10^{-2} mol/L for initiator. The linear behavior in logarithmic coordinates seen by Smith and Ewart (74) for a styrene system, which was further verified for an SBR system by Wong (70) and Broadhead (71), appears to hold (more or less) for the NBR system as well. Thus an NBR system can be considered, at least for the shown range of $[E]_o$ and $[I]_o$ (where $[E]_o$ and $[I]_o$ are the initial concentrations of emulsifier and initiator charged to the reactor), to behave according to other similar (case II kinetics) systems.

For a continuous reactor, the particle number dependence was assessed by varying the feed compositions of emulsifier and initiator as well as the mean residence time (θ) through adjustment of the total inlet flow rate to the reactor. Figure 7 reveals the influence of reactor residence time and different concentrations of emulsifier and initiator on the steady-state particle number. The base case emulsifier ($[E]_o$) and initiator ($[I]_o$) concentrations used were again set according to recipe 2 of Table 6. The response of N_p to residence time at different levels of emulsifier and initiator is consistent with simulations for SBR shown by Kanetakis et al. (75), as well as with the experimental findings of Nomura et al. (76) for styrene. Clearly, there exist certain reactor operating conditions that provide a maximum number of particles for given concentrations of emulsifier and initiator, and with no surprise equations have been proposed that predict these optimal conditions (77–78). The significance of these simulation results is to demonstrate that the current NBR model behaves according to experimental findings from other similar (case II kinetics) systems.

3.6 Continuous Reactor Start-up Procedures

To illustrate the transient behavior typically seen upon reactor start-up, the model was used to simulate two different start-up policies. The first assumes the reactor is initially full

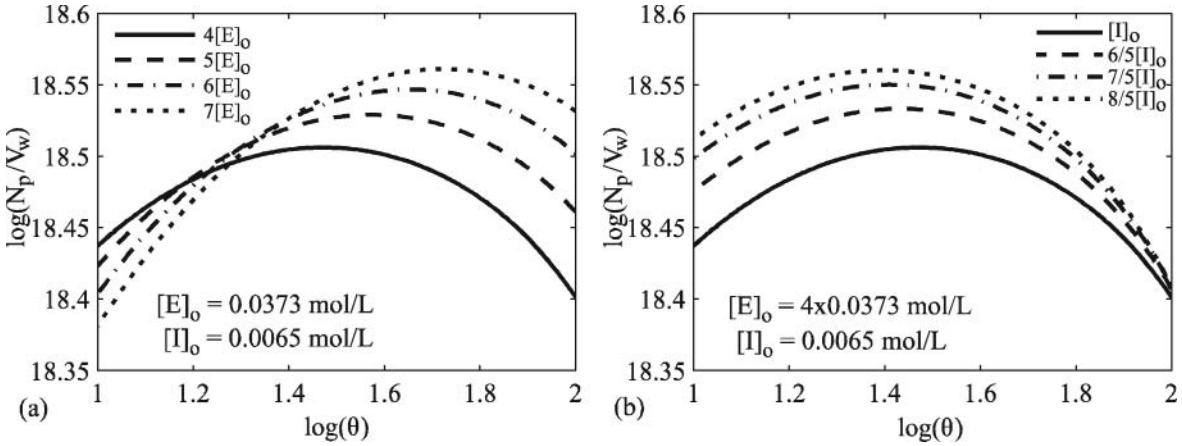

Fig. 7. NBR continuous reactor simulation of particle number (N_p) vs. mean residence time (θ) at different feed concentrations of emulsifier ($[E]_o$) (a), and initiator ($[I]_o$) (b).

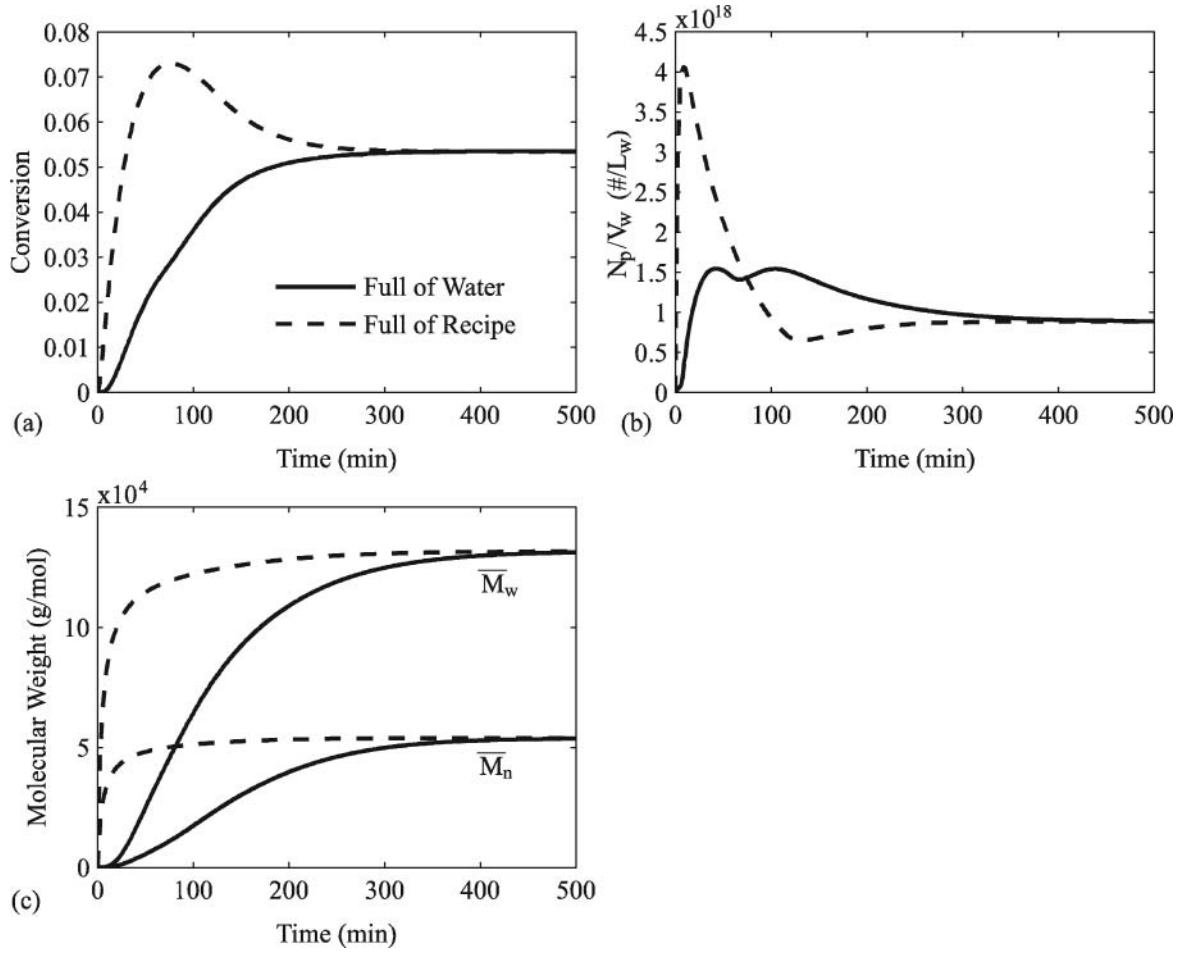

Fig. 8. Continuous reactor simulation of start-up policies for conversion, particle number, and molecular weight averages for $\theta = 60$ min.

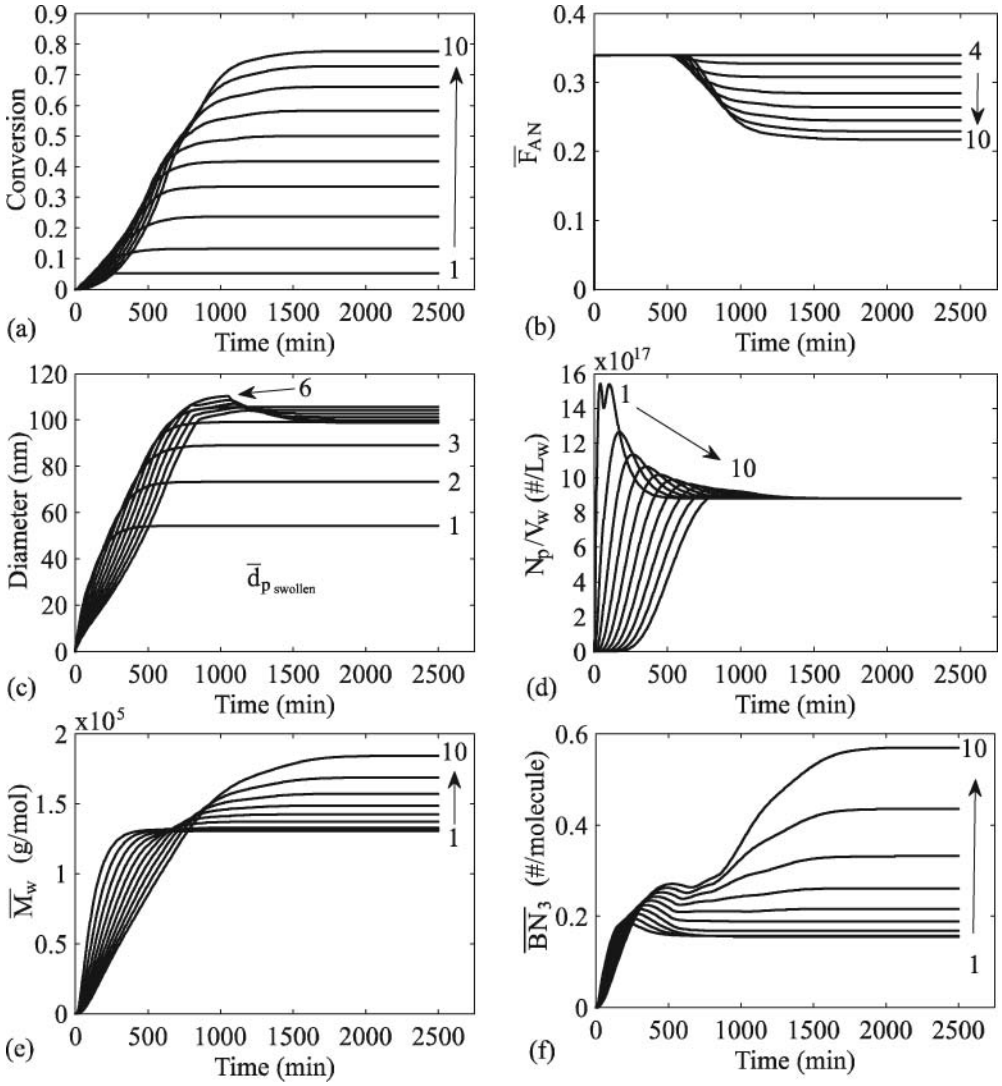

Fig. 9. Continuous reactor train simulation (recipe 1 in Table 7) for conversion (a), copolymer composition (b), average particle diameter (c), particle number (d), weight-average molecular weight (e) and tri-functional branching frequency (f).

of water, while the second considers the reactor initially full of "batch recipe" (i.e., all ingredients charged in the same proportions as in batch operation). A sample of response variables assessed includes conversion, particle number, $\bar{M}_n$ and $\bar{M}_w$, as seen in Figure 8. Using a reactor initially full of "batch recipe" reveals an initial overshoot in conversion which is due to the large initial burst in particle nucleation. Number- and weight-average molecular weights converge quickly to their steady-state values. Starting the reactor up initially full of water shows a much longer transient period in each of the reactor variables, which is to be expected.

3.7 Base Case Reactor Train Simulations

To establish a sense of the dynamic behavior of a typical NBR reactor train, a base case simulation was performed using 10 reactors each with a volume of 20000 L (typical for industrial production). A mean residence time (θ) of 60 min for each reactor was employed, which translates to a total volumetric inflow of 333 L/min to the first reactor. Similar recipe ingredient proportions to the ones used for a batch reactor (Table 6) were used for the continuous train as well, and these can be seen in Table 7. The reactor start-up procedure used was to have all reactors initially full of water before material was fed to the first reactor. The model parameters used are as stated in Appendix B.

A number of observations can be made based on the simulation results given in Figure 9. First, with the implemented start-up procedure the time to reach steady-state is 25–30 hrs for the final reactor (Fig. 9a). Starting the reactors up using a pre-emulsified solution with all recipe ingredients except for the redox agents and then feeding all recipe ingredients to the first reactor of the train, revealed a reduction of approximately 10 hours for the time

Table 7. NBR continuous process recipes

Ingredient[a]	*Recipe 1*[b]	*Recipe 2*[c]
Acrylonitrile	32	31.4
Butadiene	68	68.6
Water	180	170.2
PMHP	0.223	0.029
$FeSO_4 \cdot H_2O$	0.0056	0.0096
SFS	0.12	0.2
Dresinate	1.25	3.49
Tamol	2.85	—
Mercaptan	0.42	0.409
$q_{T_{in}}$(L/min)[d]	333	321.7[e]
Temperature (°C)	10	10

[a]In parts per hundred monomer (pphm); [b]Recipe from Dubé et al. (12); [c]Recipe from Minari et al. (16); [d]Total inlet volumetric flow to the 1st reactor; [e]An 8 reactor train was used with a volume of 17473 L per reactor ($\theta = 54.3$ min).

Table 8. Comparison of final simulated properties for the continuous process of Minari et al. (16)

Property	*This Work*[a]	*Minari et al. (16)*[b]
G (kg/min)[c]	75.6	72.2
x (%)	75.5	72.7
$N_p / V_w \times 10^{-18}$ (#/L_w)	2.18	2.48
$\bar{d}_p$(nm)	74.8	69.5
$\bar{M}_n \times 10^{-5}$ (g/mol)	0.527	0.61
$\bar{M}_w \times 10^{-5}$ (g/mol)	1.834	2.10
PDI[d]	3.48	3.44
$\overline{BN}_3$(#/molecule)	0.499	0.467
$\overline{BN}_4$(#/molecule)	0.024	—[e]
$\bar{F}_{AN}$	0.225	0.348
$\Delta \bar{F}_{AN}$(%)[f]	33.7	8.5[g]

[a]For an 8 reactor train according to recipe 2 in Table 7; [b]Simulation results reported by Minari et al. (16) for steady-state operation where all ingredients are fed to the first reactor; [c]Rate of polymer production; [d]Polydispersity ($\bar{M}_w / \bar{M}_n$); [e]Not reported; [f]Percent drift in copolymer composition; [g]Based on an initial steady-state AN composition of 37.8% in the first reactor.

to reach steady-state compared to when only water was charged to the reactor initially (not shown here for the sake of brevity). This suggests that with a carefully chosen start-up procedure and recipe and with the appropriate feed rates of recipe ingredients transient effects can be significantly reduced during start-up. This can also apply when changing polymer grade from one steady-state to another, as shown by Minari et al. (17). Other observations are that the copolymer composition begins to drift in the fourth reactor (Fig. 9b), and the monomer droplet phase vanishes in the sixth reactor which is evident from a decrease in swollen particle diameter (Fig. 9c). From Figure 9d, it can also be seen that the number of particles remains constant after the first reactor (i.e., nucleation only occurs in the first reactor). The steady-state in the first reactor is preceded by a large overshoot, where the distinct "double-hump" in N_p can be attributed to the use of two emulsifiers in the recipe. In Fig. 9e, the weight-average molecular weight appears to increase starting in the fifth reactor and continues to increase in each subsequent reactor as a result of promoted transfer to polymer and internal double bond polymerization reactions. For the same reasons, the tri-functional chain branching frequency profile (Fig. 9f) reveals a sharp increase beyond the sixth reactor, which indicates an increase in the average number of branch points per molecule, primarily due to an increase in polymer concentration in the particles after monomer droplets disappear.

3.8 Reactor Train Simulation Comparisons

Comparing the model developed in this paper with that reported by Minari et al. (16) under similar operating conditions, reveals quite similar results, despite the large number of unknowns with respect to the model parameters used by Minari et al. (16). A representative summary of these results can be seen in Table 8. Without modifying any of the database parameters, the final conversion and rate of polymer production predicted by the present model were roughly 3% higher than those reported by Minari et al. (16); N_p was slightly lower resulting in a slightly higher average diameter; both $\bar{M}_n$ and $\bar{M}_w$ as well as $\overline{BN}_3$ were in relatively good agreement. The cumulative copolymer composition, however, reveals a significant drift of approximately 33% from the first to the last reactor in the train. This behavior is strikingly different from that of Minari et al. (16) who report only an 8% drift under normal operation (i.e., all ingredients fed to the first reactor). Furthermore, using an identical monomer feed composition, the initial copolymer composition in the first reactor was approximately 4% lower than that reported by Minari et al. (16) (i.e., 34% vs. 37.8%). The higher initial copolymer composition and minimal drift reported by Minari et al. (16) is most likely a result of different partition coefficient and reactivity ratio parameters. A possible explanation for the rather small composition drift is that the initially higher copolymer composition within the particle phase is closer to the azeotropic composition which results in a lesser rate of drift. Without data to corroborate the trends of Minari et al. (16) it is difficult to comment further on the drift or lack thereof seen in each model.

3.9 Maintaining a Desired AN Copolymer Composition in a Reactor Train

Product specification is typically governed by the level of bound AN and the polymer molecular weight and branching characteristics. It is quite common in a long reactor train that intermittent additions of monomer and CTA are necessary to maintain or achieve desired polymer properties over the course of polymerization. Through simulation, it is shown in Figure 10 that simply

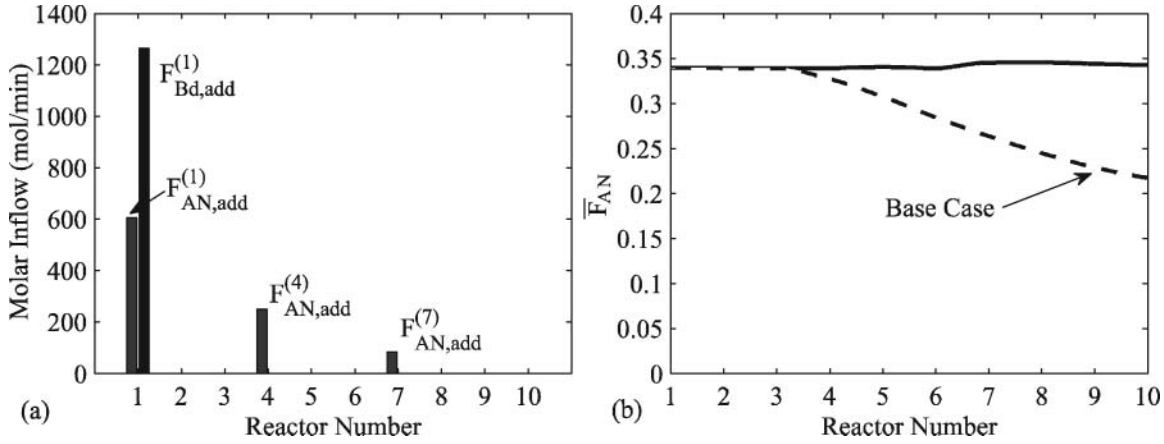

Fig. 10. Continuous NBR reactor train simulation for composition control: (a) monomer inflow, (b) cumulative AN copolymer composition.

feeding all recipe ingredients to the first reactor of the train without further additions often yields unacceptable or out-of-specification final rubber properties. Clearly seen is a large drift in copolymer composition if additional AN is not fed along the train. It should also be noted that further monomer addition can often cause the molecular weight and branching frequency to drift out of specification. Thus, controlling bound AN, molecular weight and chain branching is often a simultaneous objective in order to keep the polymer specifications on target.

3.10 Increasing Polymer Productivity in a Reactor Train

In addition to controlling the molecular characteristics (i.e., bound AN, molecular weight and chain branching), it is also often desirable to influence the rate of polymer

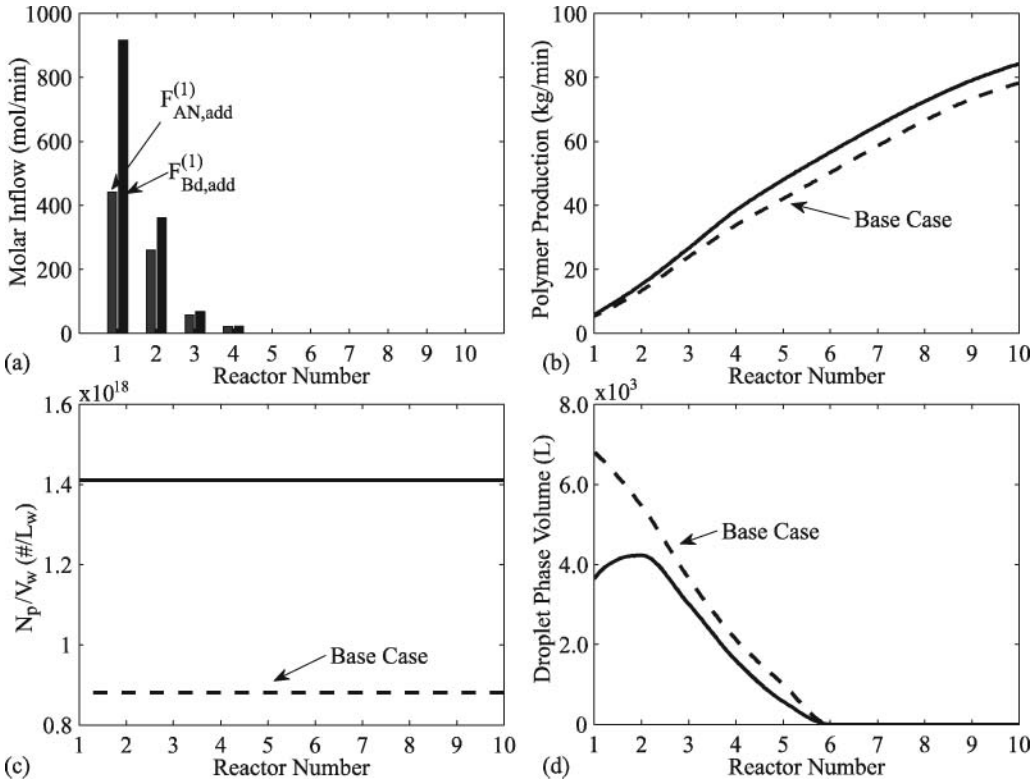

Fig. 11. Continuous NBR reactor train simulation of monomer feed policies for maximizing polymer production: (a) monomer inflow, (b) rate of polymer production, (c) number of particles per liter of water, (d) monomer droplet phase volume.

production along the reactor train. One way of increasing production involves increasing the number of particles nucleated in the first reactor of the train and distributing the monomer feed over the first few reactors in the train, thus limiting the inert droplet phase that is carried between each reactor. To demonstrate this scenario some of the monomer feed to the first reactor is diverted to downstream reactors, while all other ingredients are fed to the first reactor in their original recipe proportions but at heightened flow rates so that the original reactor residence time is maintained. It was found through simulation that a monomer split ratio between 72/28 and 62/38 (i.e., 62% to the first reactor, 38% to downstream reactors) allowed for an increase in particle nucleation, which can be attributed to the increased level of emulsifier and initiator introduced to the system. Consequently, this led to an increased polymerization rate and hence productivity.

After simulating several operating scenarios it was found that in order to increase polymer production a combination of increased particle number, additional AN to reduce composition drift, an appropriate monomer split ratio, and an appropriately selected residence time (i.e., optimal in the sense of providing maximum particle nucleation) was required. For example, Figure 11 reveals an operating strategy using a split ratio of 67/33, a residence time of 55 min in the 1st reactor and a feed policy of diverted monomer (i.e., the remaining 33%) of 80%, 15% and 5% into the 2nd, 3rd and 4th reactors, respectively. Furthermore, additional AN was introduced into the same reactors according to the percentages of 50%, 75% and 100% on top of the base feed rates for each respective reactor (see Fig. 11a). From Figure 11b it can be seen that, according to this operating policy, the rate of polymer production can be increased by approximately 6 kg/min from the base case simulation. Though this increased amount may seem insignificant from an industrial perspective, the idea of increasing productivity through a carefully chosen operating policy is evident. Figure 11c shows the increased particle number, while also apparent from Figure 11d is that the inert droplet phase was reduced and in fact, disappeared 400 min sooner in the 6th reactor than the base case simulation.

4 Conclusions

A dynamic model for emulsion polymerization capable of simulating batch, semi-batch, continuous, and trains of continuous reactors has been presented and tested against several data sets for NBR and butadiene emulsion polymerization. Model predictions for a batch reactor compared favorably to available literature data on conversion, copolymer composition, average particle diameter and molecular weights, and percent solids. Simulation studies on a train of continuous reactors proved to be comparable to those performed by Minari et al. (16). Further simulation studies highlighted the use of the model for developing optimal reactor recipes, efficient start-up policies, and operating policies for copolymer composition control (i.e., drift prevention) and increased polymer production.

References

1. Bovey, F.A., Kolthoff, I.M., Medalia, A.I. and Meehan, E.J. Emulsion Polymerization, Wiley Interscience: New York, 1955.
2. Hofmann, W. (1967) *Rubber Chem. Technol*., 37(2.2), 1–252.
3. de la Cal, J.C., Leiza, J.M., Asua, J.M., Butte, A., Storti, G. and Morbidelli, M. Emulsion Polymerization. In Handbook of Polymer Reaction Engineering, Meyer, T. and Keurentjes, J., Ed. Wiley-VCH: 249–332, 2005.
4. Dubé, M.A., Soares, J.B.P., Penlidis, A. and Hamielec, A.E. (1997) *Ind. Eng. Chem. Res*., 36(4), 966–1015.
5. Gao, J. and Penlidis, A. (2002) *Prog. Polym. Sci.*, 27(3), 403–535.
6. Saldivar, E., Dafniotis, P. and Ray, W.H. (1998) *J. Macromol. Sci., Rev. Macromol. Chem. Phys*., C38(2), 207–325.
7. Casella, E., Araujo, O. and Giudici, R. (2003) *Polym. React. Eng*., 11(4), 869–910.
8. Barclay, B., Penlidis, A. and Gao, J. (2003) *Polym. React. Eng*., 11(4), 737–814.
9. Alhamad, B., Romagnoli, J.A. and Gomes, V.G. (2005) *Chem. Eng. Sci.*, 60(10), 2795–2813.
10. Broadhead, T.O., Hamielec, A.E. and MacGregor, J.F. (1985) *Makromol. Chem*., 10(S19851), 105–128.
11. Gugliotta, L.M., Brandolini, M.C., Vega, J.R., Iturralde, E. O., Azum, J.L. and Meira, G. R. (1995) *Polym. React. Eng.*, 3(3), 201–233.
12. Dubé, M.A., Penlidis, A., Mutha, R.K. and Cluett, W.R. (1996) *Ind. Eng. Chem. Res*., 35(12), 4434–4448.
13. Vega, J.R., Gugliotta, L.M., Bielsa, R.O., Brandolini, M.C. and Meira, G.R. (1997) *Ind. Eng. Chem. Res*., 36(4), 1238–1246.
14. Rodriguez, V.I., Estenoz, D.A., Gugliotta, L.M. and Meira, G.R. (2002) I*nt. J. Polym. Mater*., 51(6), 511–527.
15. Vega, J.R., Gugliotta, L.M. and Meira, G.R. (2002) *Polym. React. Eng*., 10(1–2), 59–82.
16. Minari, R.J., Gugliotta, L.M., Vega, J.R. and Meira, G.R. (2007) *Comput. Chem. Eng.*, 31(9), 1073–1080.
17. Minari, R.J., Gugliotta, L.M., Vega, J.R. and Meira, G.R. (2007) *Ind. Eng. Chem. Res.*, 46(23), 7677–7683.
18. Asua, J.M., Sudol, E.D. and El-Aasser, M.S. (1989) J. *Polym. Sci., Part A: Polym. Chem*., 27(12), 3903–3913.
19. Hamielec, A.E. and MacGregor, J.F. Modelling Copolymerizations - Control of Composition, Chain Microstructure, Molecular Weight Distribution, Long Chain Branching and Crosslinking. In Polymer Reaction Engineering: Influence of Reaction Engineering on Polymer Properties, Reichert, K.H. and Geiseler, W., Ed. Hanser Publishers: New York, 22–71, 1983.
20. Mead, R.N. and Poehlein, G.W. (1989) *Ind. Eng. Chem. Res*., 28(1), 51–57.
21. Thickett, S.C. and Gilbert, R.G. (2007) *Polymer*, 48(24), 6965–6991.
22. Tazawa, A., Omi, S. and Kubota, H. (1972) *J. Chem. Eng. Jpn*., 5(1), 44–50.
23. Omi, S., Negishi, M., Fujitake, M. and Iso, M. (1986) *Zairyo Gijutsu*, 4(3), 130–140.
24. McCarthy, S.J., Elbing, E.E., Wilson, I. R., Gilbert, R.G., Napper, D.H. and Sangster, D.F. (1986) *Macromolecules*, 19(9), 2440–2448.
25. Nishida, R., Poehlein, G.W. and Schork, F.J. (1995) *Polym. React. Eng*., 3(4), 397–420.
26. Morton, M., Salatiello, P.P. and Landfield, H. (1952) *J. Polym. Sci.*, 8(1), 111–121.
27. Morton, M., Salatiello, P.P. and Landfield, H. (1952) *J. Polym. Sci*., 8(2), 215–224.

28. Minhas, B.S., Ph.D. Thesis, University of Ottawa, Department of Chemical Engineering, 1983.
29. Pallaske, U., Schmidt, A. and Ott, K.H. General Mathematical Model for Simulation of Dynamic Behavior of Emulsion Polymerization. In Polymer Reaction Engineering: Emulsion Polymerization, High Conversion Polymerization, Polycondensation, Reichert, K.H. and Geiseler, W., Ed. Huthig and Wepf: Verlag, Basel, Heidelberg, New York, 19–39, 1986.
30. Weerts, P.A., German, A.L. and Gilbert, R.G. (1991) *Macromolecules*, 24(7), 1622–1628.
31. Weerts, P.A., van der Loos, J.L.M. and German, A.L. (1989) *Makromol. Chem.*, 190(4), 777–788.
32. Weerts, P.A., van der Loos, J.L.M. and German, A.L. (1990) *Makromol. Chem*., 191(11), 2615–2630.
33. Weerts, P.A., van der Loos, J.L.M. and German, A.L. (1991) *Makromol. Chem*., 192(9), 1993–2008.
34. Weerts, P.A., van der Loos, J.L.M. and German, A.L. (1991) *Makromol. Chem*., 192(9), 2009–2019.
35. Deibert, S. and Bandermann, F. (1993) *Makromol. Chem*., 194(12), 3287–3299.
36. Deibert, S., Bandermann, F., Schweer, J. and Sarnecki, J. (1992) *Makromol. Chem. Rapid Commun*., 13(7), 351–355.
37. Verdurmen, E.M., Dohmen, E.H., Verstegen, J.M., Maxwell, I.A., German, A.L. and Gilbert, R.G. (1993) *Macromolecules*, 26(2), 268–275.
38. Verdurmen, E.M., German, A.L., Sudol, E.D. and Gilbert, R.G. (1994) *Macromol. Chem. Phys*., 195(2), 635–640.
39. Verdurmen, E.M., Geurts, J.M. and German, A.L. (1994) *Macromol. Chem. Phys*., 195(2), 621–633.
40. Verdurmen, E.M., Geurts, J.M. and German, A.L. (1994) *Macromol. Chem. Phys*., 195(2), 641–645.
41. Verdurmen, E.M., Geurts, J.M., Verstegen, J.M., Maxwell, I.A. and German, A.L. (1993) *Macromolecules*, 26(23), 6289–6298.
42. Verdurmen, E.M., Verstegen, J.M. and German, A.L. (1994) *Macromol. Chem. Phys*., 195(2), 647–659.
43. Wall, F.T., Powers, R.W., Sands, G.D. and Stent, G.S. (1948) *J. Am. Chem. Soc*., 70(3), 1031–1037.
44. Embree, W.H., Mitchell, J.M. and Williams, H.L. (1951) *Can. J. Chem*., 29(3), 253–269.
45. Poddubny, I.Y. and Rabinerzon, M.A. (1965) *J. Appl. Polym. Sci*., 9(7), 2527–2536.
46. Uraneck, C.A. and Burleigh, J.E. (1968) *J. Appl. Polym. Sci.*, 12(5), 1075–1095.
47. Burnett, G.M., Cameron, G.G. and Thorat, P.L. (1970) *J. Polym. Sci., Part A-1: Polym. Chem*., 8(12), 3235–3442.
48. Burnett, G.M., Cameron, G.G. and Thorat, P.L. (1970) *J. Polym. Sci., Part A-1: Polym. Chem*., 8(12), 3443–3453.
49. Burnett, G.M., Cameron, G.G. and Thorat, P.L. (1970) *J. Polym. Sci., Part A-1: Polym. Chem*., 8(12), 3455–3460.
50. Vialle, J., Guillot, J. and Guyot, A. (1972) *Rubber Chem. Technol*., 45(6), 1546–1553.
51. Guillot, J. (1981) *Acta Polym*., 32(10), 593–600.
52. Lin, C.C., Ku, H.C. and Chiu, W.Y. (1981) *J. Appl. Polym. Sci.*, 26(4), 1327–1342.
53. Guyot, A. Features of Emulsion Copolymerization of Acrylonitrile. In Polymer Reaction Engineering: Influence of Reaction Engineering on Polymer Properties, Reichert, K.H. and Geiseler, W., Ed. Hanser Publishers: New York, 287–312, 1983.
54. Guyot, A., Guillot, J., Graillat, C. and Llauro, M.F. (1984) *J. Macromol. Sci. Chem.*, A21(6–7), 683–699.
55. Hoffman, E.J., M. Eng. Thesis, McMaster University, Department of Chemical Engineering, 1984.
56. Omi, S., Negishi, M., Kushibiki, K. and Iso, M. (1985) *Makromol. Chem*., 10(S19851), 149–158.
57. Shvetsov, O. K. (1986) *Acta Polym*., 37(9), 573–577.
58. Filho, A.P., Araujo, O., Giudici, R. and Sayer, C. (2006) *Macromol. Symp*., 243(1), 114–122.
59. Dainton, F.S. and Eaton, R.S. (1959) *J. Polym. Sci*., 39(135), 313–320.
60. Garcia-Rubio, L.H., Lord, M.G., MacGregor, J.F. and Hamielec, A.E. (1985) *Polymer*, 26(13), 2001–2013.
61. Thomas, W.M. and Webb, R.L. (1957) *J. Polym. Sci.*, 25(108), 124–125.
62. Sarkar, S., Adhikari, M.S., Banerjee, M. and Konar, R.S. (1988) *J. Appl. Polym. Sci*., 36(8), 1865–1876.
63. Polymer Handbook, 4th Edition; John Wiley & Sons: New York, 1999.
64. Gugliotta, L.M., Arzamendi, G. and Asua, J.M. (1995) *J. Appl. Polym. Sci*., 55(7), 1017–1039.
65. Maxwell, I.A., Kurja, J., Van Doremaele, G.H.J. and German, A.L. (1992) *Makromol. Chem*., 193(8), 2065–2080.
66. Morton, M., Kaizerman, S. and Altier, W. (1954) *J. Colloid Interface Sci*., 9 300–312.
67. Ugelstad, J., Mork, P. C., Mfutakamba, H.R., Soleimany, E., Nordhuus, I., Schmid, R., Berge, A., Ellingsen, T., Aune, O. and Nustad, K. Thermodynamics of Swelling of Polymer, Oligomer and Polymer-Oligomer Particles. Preparation and Application of Monodisperse Polymer Particles. In Science and Technology of Polymer Colloids, Poehlein, G.W., Ottewill, R.H. and Goodwin, J.W., Ed. Martinus Nijhoff Publishers: 1, 51–99, 1983.
68. Hamielec, A.E., MacGregor, J.F. and Penlidis, A. (1987) *Makromol. Chem. Macromol. Symp*., 10/11 521–570.
69. Huo, B.P., Campbell, J.D., Penlidis, A., MacGregor, J.F. and Hamielec, A.E. (1988) *J. Appl. Polym. Sci*., 35(8), 2009–2021.
70. Wong, F.Y.C., M.Eng. Thesis, McMaster University, Department of Chemical Engineering, 1984.
71. Broadhead, T.O., M.Eng. Thesis, McMaster University, Department of Chemical Engineering, 1984.
72. Weerts, P.A., Ph.D. Thesis, Technische Universiteit Eindhoven, 1990.
73. Penlidis, A., MacGregor, J.F. and Hamielec, A.E. (1988) *J. Appl. Polym. Sci*., 35(8), 2023–2038.
74. Smith, W.V. and Ewart, R.H. (1948) *J. Chem. Phys.*, 16(6), 592–599.
75. Kanetakis, J., Wong, F.Y.C., Hamielec, A.E. and MacGregor, J.F. (1985) *Chem. Eng. Commun*., 35(1–6), 123–140.
76. Nomura, M., Kojima, H., Harada, M., Eguchi, W. and Nagata, S. (1971) *J. Appl. Polym. Sci*., 15(3), 675–691.
77. Hamielec, A.E. and MacGregor, J.F. Latex Reactor Principles: Design, Operation, and Control. In Emulsion Polymerization, Piirma, I., Ed. Academic Press: New York, 1982.
78. Nomura, M. On the Optimal Reactor Type and Operation for Continuous Emulsion Polymerization. In Emulsion Polymers and Emulsion Polymerization, Bassett, D.R., Ed. American Chemical Society: 121–143, 1981.
79. Washington, I.D., M.A.Sc. Thesis, University of Waterloo, Department of Chemical Engineering, 2008.

Appendix A

This Appendix provides further details on all state equations, model outputs, and other algebraic equations used in the model. For the interested reader, further details can be found in (79).

Summary of the Mathematical Model

State Equations

The model states are described by the following ODEs:

Initiator (I)	$\frac{d}{dt}(N_I) = F_{I_{in}} - F_I - R_{I_c} V_a$
Redox ingredients (RA, Fe, Fe^{2+}, Fe^{3+})	$\frac{d}{dt}(N_{RA}) = F_{RA_{in}} - F_{RA} - R_{RA} V_a$ $\frac{d}{dt}(N_{Fe}) = F_{Fe_{in}} - F_{Fe}$ $\frac{d}{dt}(N_{Fe^{2+}}) = F_{Fe^{2+}_{in}} - F_{Fe^{2+}} - R_{Fe^{2+}} V_a$ $\frac{d}{dt}(N_{Fe^{3+}}) = F_{Fe^{3+}_{in}} - F_{Fe^{3+}} - R_{Fe^{3+}} V_a$
Monomer (M)	$\frac{d}{dt}(N_{m_j}) = F_{m_{j_{in}}} - F_{m_j} - (R_{p_{j_p}} V_p + R_{p_{j_a}} V_a)$
Bound monomer (POL)	$\frac{d}{dt}(N_{pol_j}) = F_{pol_{j_{in}}} - F_{pol_j} + (R_{p_{j_p}} V_p + R_{p_{j_a}} V_a)$
Aqueous phase monomer	$\frac{d}{dt}(N_{m_{j_a}}) = F_{m_{j_{a_{in}}}} - F_{m_{j_a}} - \text{transfer}_j$
Water (W)	$\frac{d}{dt}(N_w) = F_{w_{in}} - F_w$
Emulsifier (E)	$\frac{d}{dt}(N_{e_j}) = F_{e_{j_{in}}} - F_{e_j}$
Water-soluble impurities (WSI)	$\frac{d}{dt}(N_{wsi_j}) = F_{wsi_{j_{in}}} - F_{wsi_j} - R_{wsi_{j_a}} V_a$
Monomer-soluble impurities (MSI)	$\frac{d}{dt}(N_{msi_j}) = F_{msi_{j_{in}}} - F_{msi_j} - R_{msi_{j_p}} V_p$
Chain transfer agent (CTA)	$\frac{d}{dt}(N_{cta_j}) = F_{cta_{j_{in}}} - F_{cta_j} - R_{cta_{j_p}} V_p$
Number of particles	$\frac{d}{dt}(N_p) = F_{p_{in}} - F_p + (R_{mic} + R_{hom}) V_a$
Particle phase volume	$\frac{d}{dt}(V_p) = q_{p_{in}} - q_p + \text{growth}$
MWD moments	$\frac{d}{dt}(V_p Q_i) = F_{(V_p Q_i)_{in}} - F_{V_p Q_i} + R_{V_p Q_i} V_p$
Branching averages	$\frac{d}{dt}(V_p Q_0 \overline{BN}_i) = F_{(V_p Q_0 \overline{BN}_i)_{in}} - F_{V_p Q_0 \overline{BN}_i} + R_{V_p Q_0 \overline{BN}_i} V_p$

Component balances were performed on a mole basis, j corresponds to multiple components of emulsifier, CTA, monomer, etc., i corresponds to moments 0, 1, 2 or tri- or tetra-functional branching frequencies depending on the context and N_p is expressed in # of particles.

Output Equations

Conversion	$x = \sum_i^{N_m} \left(\frac{N_{pol_i} MW_{m_i}}{\sum_j^{N_m} \left(N_{pol_j} + N_{m_j} \right) MW_{m_j}} \right)$
Percent solids	$\%\ \text{solids} = \left(\frac{\sum_j^{N_m} M_{pol_j}}{\sum_j^{N_m} \left(M_{m_j} + M_{pol_j} \right) + M_w + \sum_j^{N_{em}} M_{e_j}} \right) \times 100$
Cumulative copolymer composition	$\bar{F}_{AN} = \frac{N_{pol_A}}{\sum_j^{N_m} N_{pol_j}}$
Average particle diameter (dm)	$\bar{d}_p = \begin{cases} \left(\frac{6 V_p}{\pi N_p} \right)^{1/3} & \text{swollen} \\ \left(\frac{6 V_p \phi_p^p}{\pi N_p} \right)^{1/3} & \text{unswollen} \end{cases}$
Number-average molecular weight (g/mol)	$\bar{M}_n = M_{\text{eff}} \frac{V_p Q_1}{V_p Q_0}$
Weight-average molecular weight (g/mol)	$\bar{M}_w = M_{\text{eff}} \frac{V_p Q_2}{V_p Q_1}$
Tri-functional branching frequency (#/molecule)	$\overline{BN}_3 = \frac{V_p Q_0 \overline{BN}_3}{V_p Q_0}$
Tetra-functional branching frequency (#/molecule)	$\overline{BN}_4 = \frac{V_p Q_0 \overline{BN}_4}{V_p Q_0}$

The indices i and j correspond to component type (i.e., monomer A and B, or emulsifier 1 and 2, etc.).

Rate/Concentrations/Flow Rates

Species consumption/generation rates associated with the previously stated component balances and the corresponding phase concentrations and molar flow rates of each species can be defined as follows:

Rate of initiator consumption [a]	$R_{I_c} = k_1[I]_a[Fe^{2+}]_a + k_d[I]_a$
Rate of redox reactions	$R_{RA} = k_2[RA]_a[Fe^{3+}]_a$ $R_{Fe^{2+}} = k_1[I]_a[Fe^{2+}]_a - k_2[RA]_a[Fe^{3+}]_a$ $R_{Fe^{3+}} = -R_{Fe^{2+}}$
Rate of polymerization	$R_{p_{j_k}} = [R^{\cdot}]_k[M]_k f_{j_k} \sum_i^{N_m} (k_{p_{i_{j_k}}} \phi^{\cdot}_{i_k})$
Rate of CTA consumption	$R_{cta_{j_p}} = [R^{\cdot}]_p[CTA]_p f_{cta_{j_p}} \sum_i^{N_m} (k_{fcta_{i_{j_p}}} \phi^{\cdot}_{i_p})$
Rate of WSI consumption	$R_{wsi_{j_a}} = [R^{\cdot}]_a[WSI]_a f_{wsi_{j_a}} \sum_i^{N_m} (k_{fwsi_{i_{j_a}}} \phi^{\cdot}_{i_a})$
Rate of MSI consumption	$R_{msi_{j_p}} = [R^{\cdot}]_p[MSI]_p f_{msi_{j_p}} \sum_i^{N_m} (k_{fmsi_{i_{j_p}}} \phi^{\cdot}_{i_p})$
Rate of Q_0 generation	$R_{V_p Q_0} = \left(\tau + \frac{\beta}{2} - \frac{(C_{p^*} V_p Q_0 + C_{p^{**}} V_p Q_1)}{V_p[M]_p}\right) k_p[M]_p[R^{\cdot}]_p$
Rate of Q_1 generation	$R_{V_p Q_1} = \gamma k_p[M]_p[R^{\cdot}]_p$
Rate of Q_2 generation	$R_{V_p Q_2} = \left(\gamma + 2\left(1 + \frac{C_{p^*} V_p Q_1 + C_{p^{**}} V_p Q_2}{V_p[M]_p}\right)\frac{\xi}{\lambda} + \beta\left(\frac{\xi}{\lambda}\right)^2\right) k_p[M]_p[R^{\cdot}]_p$
Rate of $\overline{BN}_3$ generation	$R_{V_p Q_0 \overline{BN}_3} = \left(\frac{C_{fp} V_p Q_1 + C_{p^*} V_p Q_0}{V_p}\right) k_p[R^{\cdot}]_p$
Rate of $\overline{BN}_4$ generation	$R_{V_p Q_0 \overline{BN}_4} = \frac{C_{p^{**}} V_p Q_1}{V_p} k_p[R^{\cdot}]_p$
Concentration of I, RA, E, WSI	$[i]_a = \frac{N_i}{V_a}$
Concentration of CTA, MSI	$[i]_p = \frac{N_i}{V_p + V_d K_i^{d/p}}$
Aqueous phase radical concentration	$[R^{\cdot}]_a = [R^{\cdot}_{in}]_a + \sum_{i=1}^{N_m} \sum_{k=1}^{j_{cr}-1} [R_{k,i}]_a$
Particle phase radical concentration	$[R^{\cdot}]_p = \frac{\bar{n} N_p}{V_p N_A}$
Concentration of monomer i in phase k	$[M_i]_k = \phi^k_{m_i} \frac{MW_{m_i}}{\rho_{m_i}}$
Rate of monomer j transfer	$\text{transfer}_j = \begin{cases} 0 & \text{if } V_d > 0 \\ R_{p_{j_a}} V_a & \text{otherwise} \end{cases}$
Total rate of volume growth	$\text{growth} = \begin{cases} \sum_i^{N_m} \frac{MW_{m_i}\left(R_{p_{i_a}} V_a + R_{p_{i_p}} V_p\right)}{\phi^p_p \rho_p} & \text{if } V_d > 0 \\ \sum_i^{N_m} \frac{MW_{m_i} R_{p_{i_a}} V_a}{\rho_p} - \sum_i^{N_m} MW_{m_i} R_{p_{i_p}} V_p \left(\frac{1}{\rho_{m_i}} - \frac{1}{\rho_p}\right) & \text{otherwise} \end{cases}$
Total rate of volume shrinkage	$\text{shrinkage} = \sum_i^{N_m} MW_{m_i}\left(R_{p_{i_a}} V_a + R_{p_{i_p}} V_p\right)\left(\frac{1}{\rho_{m_i}} - \frac{1}{\rho_p}\right)$
Total volumetric flow rate	$q_T = q_{T_{in}} - \text{shrinkage}$
Volumetric flow rate for phase k	$q_k = \frac{V_k}{V_T} q_T$
Total molar outflow rate for species i	$F_i = \sum_k^P [i]_k q_k$
Total inflow of species i to reactor r	$F^{(r)}_{i_{in}} = F_i^{(r-1)}$

[a] This is not equivalent to the rate of initiation $R_I = k_1[I]_a[Fe^{2+}]_a + 2fk_d[I]_a$.

where $[\cdot]_k$ denotes species concentrations in either the aqueous or particle phases, f_{j_k} represents the mole fraction of monomer j in phase k and similarly for CTA, WSI and MSI, $\phi^{\cdot}_{i_k}$ corresponds to the mole fraction of radical i in phase k, and $\phi^k_{m_i}$ represents the volume fraction of monomer i in phase k.

Other Algebraic Equations

Auxiliary equations used in the previously stated reaction rates and concentrations are defined as follows:

Moles of particle phase monomer	$N_{m_{i_p}} = \begin{cases} \frac{N_{m_{i_a}} V_p}{K_i^{a/p} V_a} & \text{if } N_{m_{i_d}} > 0 \\ N_{m_i} - N_{m_{i_a}} & \text{otherwise} \end{cases}$
Moles of droplet phase monomer	$N_{m_{i_d}} = N_{m_i} - N_{m_{i_a}} - N_{m_{i_p}}$
Radical concentration of initiator	$[R_{in}]_a = \frac{R_I}{\sum_i^{Nm} k'_{p_{i_a}} [M_i]_a + k_{fwsi} [WSI]_a}$
Radical concentration of length $k = 1$ ending in monomer i	$[R_{1,i}]_a = \frac{R_{des} + k'_{p_{i_a}} [R_{in}]_a [M_i]_a}{\sum_j^{Nm} k_{p_{ij_a}} [M_j]_a + k_{t_a} [R]_a + k_{fwsi} [WSI]_a}$
Radical concentration of length $k \geq 2$ ending in monomer i	$[R_{k,i}]_a = \frac{\sum_j^{Nm} k_{p_{jia}} [R_{k-1,j}]_a [M_i]_a}{\sum_j^{Nm} k_{p_{ij_a}} [M_j]_a + k_{t_a} [R]_a + k_{fwsi} [WSI]_a + \text{capture}}$
	$\text{capture} = \begin{cases} 0 & \text{for } 2 \leq k \leq j_{cr}/2 \\ k_{cm} A_m / V_a + k_{cp} A_p / V_a & \text{for } j_{cr}/2 + 1 \leq k \leq j_{cr} - 1 \end{cases}$
Total particle surface area	$A_p = (36\pi N_p)^{1/3} V_p^{2/3}$
Total free-micellar area	$A_m = \sum_i^{N_{em}} (S_{a_i} ([E_i]_a - CMC_i) V_a N_A) - A_p$
Termination rate constant	$k_{t_p} = k_{t_{0_p}} \exp(A_1 X + A_2 X^2 + A_3 X^3)$
	$X = \begin{cases} x_c & \text{if } V_d > 0 \\ x & \text{otherwise} \end{cases}$
	$k_{td} = \gamma_t k_{t_p}$
	$k_{tc} = (1 - \gamma_t) k_{t_p}$
Homogeneous nucleation coefficient	$H = \frac{k_h}{k_{h_0}} V_a$
Radical "gain" coefficient	$\alpha = \frac{k_{cp} A_p ([R]_a^{par} + [R]_a^{des}) V_p N_A^2}{k_{t_p} N_p^2}$
Radical "loss" coefficient	$p = \frac{(k_{des} + k_{fmsi_p} [MSI]_p) V_p N_A}{k_{t_p} N_p}$
Other groupings	$\tau = \frac{k_{td} [R]_p}{k_p [M]_p} + C_{fm} + C_{fcta} \frac{[CTA]_p}{[M]_p} + C_{fmsi} \frac{[MSI]_p}{[M]_p}$
	$\beta = \frac{k_{tc} [R]_p}{k_p [M]_p}$
	$\gamma = 1 + C_{fm} + C_{fcta} \frac{[CTA]_p}{[M]_p} + C_{fmsi} \frac{[MSI]_p}{[M]_p}$
	$\lambda = \tau + \beta + C_{fp} \frac{V_p Q_1}{V_p [M]_p}$
	$\xi = \gamma + C_{p^*} \frac{V_p Q_1}{V_p [M]_p} + \left(C_{fp} + C_{p^{**}}\right) \frac{V_p Q_2}{V_p [M]_p}$

$\tau, \beta, \gamma, \lambda, \xi$ are dimensionless group terms used in the moment equations. Note, $[R_{k,B}]_a$ is always considered zero for $k > j_{cr}/2$. An expression similar to Equation 10 for $[R]_a^{par}$ can be easily derived and is not repeated here. Further details on the formulation of $[R]_a^{des}$ and k_{des} can be found in (4-5, 79).

Appendix B

The parameters used in this paper are listed in Table B. 1. Additional information can be found in (12, 79).

Database items for the NBR model.

Parameter[a]	*Value*	*Unit*	*Source*
ε	4.839	—	This work
k_{cp}	0.025	dm/min	This work
μ	5.5×10^5	—	This work
L	1.0×10^{-4}	dm	(12)
j_{cr_A}	30	—	(12)
j_{cr_B}	5	—	(12)
x_c	0.48	—	(12)
$K_A^{a/p}$	0.75	—	(12)
$K_B^{a/p}$	0.0025	—	(12)
$K_{CTA}^{d/p}$	1.5	—	(12)
CMC (Tamol)	9.0×10^{-3}	mol/L	(12)
CMC (Dresinate)	1.0×10^{-3}	mol/L	(12)
S_a(Tamol)	6.0943×10^{-17}	dm^2/molecule	(12)
S_a(Dresinate)	4.37×10^{-17}	dm^2/molecule	(12)
r_{mic}	7.5×10^{-8}	dm	(12)
k_1	$3.78 \times 10^{11}\exp(-11100/RT)$	L/mol/min	(12)
k_2	2.5	L/mol/min	(12)
k_d	$2.8 \times 10^{18}\exp(-33500/RT)$	L/mol/min	(12)
f	0.7	—	(12)
r_A	0.05	—	(12)
r_B	0.35	—	(12)
$k_{p_{AA}}$	$6.282 \times 10^9\exp(-7278.38/RT)$	L/mol/min	(12)
$k_{p_{BB}}$	$7.2 \times 10^9\exp(-9300/RT)$	L/mol/min	(12)
$k_{t_{AA_a}}$	$1.603 \times 10^{16}\exp(-5400/RT)$	L/mol/min	(12)
$k_{t_{0_p}}$	9.0×10^4	L/mol/min	(12)
γ_t	0.55	—	(12)
A_1, A_2, A_3	−0.44, −6.75, −0.35	—	(12)
$k_{fm_{AA}}$	$6.55 \times 10^7\exp(-10972.37/RT)$	L/mol/min	(12)
$k_{fm_{BB}}$	$5.278 \times 10^8\exp(-12993.98/RT)$	L/mol/min	(12)
$k_{fm_{AB}}$	0	L/mol/min	Assumed
$k_{fm_{BA}}$	0	L/mol/min	Assumed
$k_{fp_{AA}}$	0.3	L/mol/min	This work
$k_{fp_{BB}}$	$3.969 \times 10^8\exp(-12470.6/RT)$	L/mol/min	(12)
$k_{fp_{AB}}$	$3.969 \times 10^8\exp(-12470.6/RT)$	L/mol/min	(12)
$k_{fp_{BA}}$	0.3	L/mol/min	This work
$k^*_{p_{AA}}$	0	L/mol/min	Assumed
$k^*_{p_{BB}}$	0	L/mol/min	Assumed
$k^*_{p_{AB}}$	0	L/mol/min	Assumed
$k^*_{p_{BA}}$	0	L/mol/min	Assumed
$k^{**}_{p_{AA}}$	0	L/mol/min	Assumed
$k^{**}_{p_{BB}}$	$8.1 \times 10^8\exp(-14150/RT)$	L/mol/min	(12)
$k^{**}_{p_{AB}}$	$8.1 \times 10^8\exp(-14150/RT)$	L/mol/min	(12)
$k^{**}_{p_{BA}}$	0	L/mol/min	Assumed
k_{fcta_A}	$21 \times k_{p_{AA}}$	L/mol/min	This work
k_{fcta_B}	$1.53 \times 10^7\exp(-6400/RT)$	L/mol/min	This work

[a] A stands for AN and B for Bd.